Climate Effects of Managed Boreal Forests

Combining Effects from Carbon Balance and Albedo

Anna Valeria Requardt

Climate Effects of Managed Boreal Forests - Combining Effects from Carbon Balances and Albedo.

Anna Valeria Requardt

Abstract

Boreal forests are considered as a global carbon (C) sink and are utilized for climate-change mitigation. Judging the climate impact of a forest solely on its C balance might leave an incomplete picture, since forest-climate feedbacks are also caused by various other biophysical and biogeochemical processes, e.g., albedo effects. Previous research showed a high importance of albedo effects in the boreal zone compared to other biomes, mainly due to the presence of snow.

This study quantifies the net climate effect of a forest in boreal North Sweden by considering its C and albedo dynamics. For this purpose, remotely sensed high spatial resolution albedo and ground-based C balance data were combined into a radiative forcing (RF) model. The results suggest a distinct age-related albedo pattern and the possibility of using age as a proxy for successional biophysical changes in the forest landscape. Moreover, C-flux-induced climate cooling (75% of total RF) was found to overrule albedo-induced warming (25% of total RF), which challenges previous research. The findings point towards the need for biome-specific forest management practices to yield maximum climate cooling potentials.

Table of contents

List of Tables

List of Figures

Abbreviations

Acronym	Definition	Unit
General terms		
KC	Krycklan Catchment	-
KCS	Krycklan Catchment Study	-
ICOS	Integrated Carbon Observation System	-
CC	Climate Change	-
C	Carbon	-
CO_2	Carbon Dioxide	-
BVOC	Biogenic volatile organic compounds	-
SOA	Secondary organic aerosols	-
GEE	Google Earth Engine	-
Carbon fluxes		
NEP	Net Ecosystem Production	$g\ C\ m^{-2}\ yr^{-1}$
NPP	Net Primary Production	$g\ C\ m^{-2}\ yr^{-1}$
RH	Total Heterotrophic Respiration	$g\ C\ m^{-2}\ yr^{-1}$
AGB	Aboveground Biomass	$Mg\ ha^{-1}$
ANPP	Net Primary Production of aboveground biomass	$g\ C\ m^{-2}\ yr^{-1}$
BNPP	Net Primary Production of belowground biomass	$g\ C\ m^{-2}\ yr^{-1}$
LAI	Leaf Area Index	$m^2\ m^{-2}$
SDS	Stand age class	-
SPM	Dominant tree species	-
Radiative Forcing		
RF	Radiative Forcing	$W\ m^{-2}$
RE	Radiative Efficiency	$W\ m^{-2}\ kg^{-1}$

τ	Residence time	yrs
f_i	Fraction multiplier	
ϕ_i	Net CO_2 flux into atmosphere	g CO_2 m^{-2} yr^{-1}
t	time	yrs
S	Surface area	m^2

Albedo

α_λ	Spectral (narrowband) Blue-Sky Albedo	-
A	Broadband Albedo	-
BRDF	Bidirectional reflectance distribution function	-
BSA	Black-Sky Albedo	-
WSA	White-Sky Albedo	-
SW	Shortwave spectrum	nm
RGB	Blue, Green, and Red Spectrum	nm
VIS	Visible Spectrum	nm
MODIS	MODerate-resolution Imaging Spectroradiometer	-
S2	Sentinel-2	-
AN ratio a	Albedo to near-nadir reflectance ratio	-
$\bar{a}$	BSA to near-nadir reflectance ratio	-
$\bar{\bar{a}}$	WSA to near-nadir reflectance ratio	-
λ	Spectral band	-
Ω_{S2}	S2 sun-view geometry	rad
θ_s	Solar zenith angle of S2	rad
θ_v	View zenith angle of S2	rad
R	Bidirectional reflectance	rad^{-1}
β	Diffuse sunlight fraction	-
$f_{iso}, f_{vol}, f_{geo}$	Isometric, volumetric, and geometric weighting parameters from the MODIS BRDF product	-

$h_{vol}, h_{geo}, h_{iso}$	Approximation for the volumetric, isometric, and geometric BRDF kernels	-
$H_{iso}, H_{vol}, H_{geo}$	WSA integrals of kernel approximations	-
c_i	Narrow-to-broadband conversion coefficient	-
Statistics		-
PCA	Principal Component Analysis	-
RMSE	Root Mean Square Error	-

Introduction

1.1 The role of boreal forests in the climate system

Forest-climate feedbacks are caused by biophysical and biogeochemical processes that directly or indirectly influence radiative forcing (Anderson et al. 2011; Kirschbaum et al. 2011). Radiative forcing (RF) describes variations in energy fluxes of the earth's atmosphere and is measured in watts per square meter (IPCC, 2007). In climate change research, RF quantifies the impact of external factors such as greenhouse gas emissions or land use change, e.g., forest management, on earth's energy balance (IPCC, 2007). A positive radiative forcing refers to more incoming than outgoing energy on a planetary level, meaning a warming effect (here referred to as 'climate warming'). A negative radiative forcing means more outgoing than incoming energy, thus a cooling effect (here referred to as 'climate cooling').

A variety of biogeochemical and biophysical processes can influence the effect of forests on the planet's radiative forcing. Within that, climatic impacts of forests are mainly judged by their C sequestration potential whilst other climate relevant effects are largely ignored (Anderson et al., 2011). Boreal forests are storing around 33% of the global carbon (C) pool (Pan et al. 2011) and are important climate change (CC) mitigation tools (UNFCC, 2016). Due to their C sequestration potential, boreal forests are considered to serve as sinks of atmospheric carbon dioxide (CO_2) (Myneni et al. 2001). However, the CO_2 sink strength depends on the stand age (Coursolle et al. 2012; Besnard et al. 2018; Peichl et al. 2023a), nutrient availability in soils (Janssens et al. 2010; Vicca et al. 2012; Fernández-Martínez et al. 2014), climate (Coursolle et al. 2012) and species (Curtis & Gough 2018). Within this variability, clear-cut and mature boreal forests can even function as a CO_2 source (Hadden & Grelle 2016; Lindroth et al. 2020; Vestin et al. 2020). A previous study by Peichl et al. (2023a) in the same Swedish boreal forest catchment used in this work shows an influence of the stand age on the sink effect of atmospheric C, with young and very old stands having a lower C sequestration potential than middle-aged stands.

Apart from C sequestration, multiple biophysical processes also have non-negligible climate impacts and can either cool or warm the atmosphere (Anderson et al. 2011, Figure 1). Examples thereof are a) evapotranspiration and feedbacks

with cloud formation and precipitation (Xu et al., 2022; Zhao et al. 2017), b) forest-aerosol-feedbacks like the emission of biogenic volatile organic compounds (BVOC) and secondary organic aerosols (SOA) (Kulmala et al. 2004), and c) surface reflectance effects from forest canopies (Anderson et al. 2011).

The latter is also called albedo feedback, with the albedo (A) defined as the ratio of incoming to reflected solar radiation (Burakowski et al. 2015). The lower the albedo of a surface, the more solar radiation energy is absorbed and can contribute to surface warming. Albedo characteristics of surfaces highly depend on the surface colour and structure, e.g., the vegetation canopy (Bright et al. 2015). Forest canopies generally absorb more solar radiation than their bare underground or open landscapes due to their darker colour and surface roughness (Betts, 2000). This means that – relative to unforested areas – forests have a lower albedo and thus a climate warming effect in this aspect (Bonan 2008), which can counter the biogeochemical climate cooling effect. Ignoring those biophysical impacts might result in less effective CC mitigation measures, since they can affect the regional climate more strongly than C sequestration – sometimes even in contradicting ways (Jackson et al., 2008).
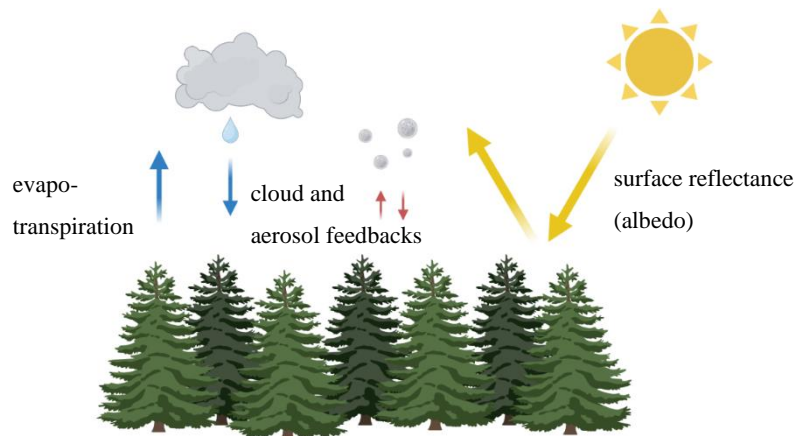
Figure 1: Forest-climate feedbacks apart from C-sequestration: evapotranspiration, cloud feedbacks, aerosol feedbacks and surface reflectance (conceptualizes as albedo). Source: own image, created with BioRender©.

A large proportion of studies focus on C sequestration of forests as the main climate impact. Whilst this is an important part to study, it is crucial to consider other radiative and non-radiative aspects of forest-climate feedbacks (Anderson et al. 2011; Bright et al. 2015). Apart from net climate effects research is in its early

stages with many research gaps (Anderson et al. 2011), especially the boreal zone of Fennoscandia remains understudied. Current research focuses more on boreal Canada and Russia, studying C balances under natural disturbances (Bond-Lamberty et al. 2004; Amiro et al. 2006; Virkkala et al. 2022). Boreal Fennoscandia is an especially important area to be studied because a) opposing climate effects of C sequestration and of albedo are especially high in this region (see section 1.3), creating large uncertainties in net climate forcing of those forests (Bonan 2008) and b) the more actively managed forests differs strongly from those in other boreal zones, consequently do net climate effects too. Management mainly consists of rotational forestry which follows a regime of clear-cutting, regeneration via natural or planted tree seedlings, and thinning (Felton et al. 2020). This type of management creates a spatially heterogeneous landscape which is characterized by even-aged stands of different age classes (Peichl et al. 2023a). This heterogeneity also creates a spatial variation in net climate effects resulting from, e.g., different C balances or albedo, since each age class has distinct C cycles and surface structures. In comparison to extensive management, this creates uncertainties about the radiative forcing effect of managed boreal forests, leaving a gap in understanding their role in earth's climate system.

1.2 Albedo effects of boreal forests and net radiative forcing

In several biomes (e.g., the tropics) biophysical effects like albedo often align with C sequestration effects to cool climate, but this is not the case within the boreal biome, where those factors often counteract (Jackson et al. 2008). There, albedo effects have a relatively higher importance compared to other biomes (Anderson et al., 2011). This is caused by snow masking effects of forests on the one hand (Bonan 2008; Anderson et al. 2011) and lower C storage rates on the other hand (Jackson et al. 2008). In the boreal winter, forest canopies cover the snow and thus have a darker surface with a lower albedo compared to open spaces like tundra (Bonan 2008).

Consequently, afforestation in the boreal biome can have relative warming effect: the higher albedo of a forested area compared to tundra can counter the C sequestration effects (Bonan 2008; Anderson et al. 2011; Mykleby et al. 2017). E.g., replacing cropland with forests in Northern Europe causes a lower albedo which can be equivalent to an emission of 60 t C ha^{-1} for a period of 20 years, which is 50% of the sequestration potential for that time period (Betts et al. 2000). Similarly, deforestation can have a relative cooling effect because the albedo increase from

deforestation can counter the CO_2 emissions caused thereby (Bonan 2008; Jackson et al. 2008).

The snow masking effect also leads to higher albedo differences between forested and non-forested areas in the boreal compared to other biomes (Li et al. 2015). Also, seasonal variations between albedos are higher in boreal regions due to a relatively higher albedo in the winter because of a snow-covered landscape (Li et al. 2015). Due to the relative importance of the albedo, the overall biophysical climate feedbacks are stronger than in any other biome (Bonan 2008). E.g., evapotranspiration cooling of forests can be outweighed completely by albedo warming (Li et al. 2015).

Not only albedo effects themselves, but also albedo estimations come with uncertainties. Deriving albedo from remote sensing offers an opportunity to create high-resolution data over larger areas (Li et al. 2018), though those Remote Sensing methods remain heavily understudied for fine-scale applications. Thus, the present study explores one of those evolving remote sensing methods to estimate high-resolution albedo data.

In the future the albedo will play an even bigger role in the boreal biome: modelling shows that this relative albedo warming effect will be amplified by climate change in the Scandinavian mountains (Wramneby et al. 2010). The distinct pattern and relatively high (future) importance of albedo effects in the boreal biome makes this aspect especially important to study when considering a boreal area.

However, net climate effects of forests also highly depend on factors like species and management (Anderson et al. 2011; Lukes et al. 2013; Kellomäki et al. 2021), stand density (Mykleby et al. 2017), stand biomass (Lukes et al. 2013) and canopy density (Lukes et al. 2013; Bright et al. 2015) as well as stand age (Bonan 2008) and harvest level (Kalliokoski et al. 2020). In a study on Finnish retention forestry, C sequestration had a higher relative contribution to the radiative forcing compared to albedo effects (Kalliokoski et al. 2020). A North American study shows that with reducing stand density, C sequestration effects decrease at higher rates than biophysical warming effects do, so there is a threshold density where forests no longer provide net cooling (Mykleby et al. 2017). Similarly, albedo values are lower with higher stand biomass (Lukes et al. 2013). Comparable to stand density also canopy density influences net climate effects, mainly due to changing vegetation structure with changing canopy densities (Bright et al. 2015). This is shown for rotation forestry, where albedo changes after a clear-cut can be persistent until the new canopy closes (Bright et al. 2015). However, the influence of canopy density on albedo varies seasonally, with a stronger influence in snow-periods compared to non-snow-periods (Ni & Woodcock 2000), mainly due to the snow-masking effect described earlier. Simulations from Finland show that non-managed forests have a climate cooling potential due to high carbon stock potentials, whilst management with even-aged and uneven-aged stands show a net-zero climate effect with albedo

and C sequestration effects levelling each other out – mainly due to relatively lower carbon stock potentials in managed forests (Kellomäki et al. 2021). Also, different tree species have a different vegetation structure and thus produce different biophysical climate effects (Bright et al. 2015). A study from Finland suggests declining albedo with stand age for coniferous forests (Kuusinen et al. 2014). However, this aspect remains understudied in Fennoscandia. This is why the present study considers the dependencies of albedo on stand ages.

Previous research shows that biophysical aspects like albedo can highly impact regional climate and that solely studying C sequestration potentials of forests is not sufficient since it neglects more complex net climate impacts. For a long time, biophysical considerations remained underrepresented in forest-climate-models (Bonan 2008) and in climate policy (Anderson et al. 2011). Research on forests net climate effects is evolving but remains understudied – especially for managed boreal landscapes of Scandinavia. Given the relatively high importance of albedo effects in this biome, this study aims to fill the research gap by estimating net climate effects via albedo and C balances of a managed boreal forest in Northern Sweden.

1.3 Study aim, objectives, and hypothesis

To fill the research gaps (see 1.1 and 1.2) this study investigated the net climate effects of a boreal area which remains understudied in comparison to other boreal zones. The aim was to determine the integrated net climate impact from albedo and C sequestration effects for a managed boreal forest landscape under rotational forestry in Northern Sweden.

The research objectives were to:
1. explore remote sensing as a tool for estimating high spatial resolution albedo over boreal catchments,
2. determine landscape variations of albedo and net climate effects within the catchment (i.e., across 50 stands differing in age and dominating tree species),
3. explore the relative importance of C sequestration vs. albedo in determining the net climate impact,
4. determine at which stand age the net climate effect is most beneficial and,
5. scale the data to understand the integrated net climate effect of the entire Krycklan catchment.

To achieve this, albedo values of different stands within the study area were retrieved and combined with C sequestration values studied by Peichl et al. (2023a)

in an integrated radiative forcing model to estimate net climate effects over the years 2016-2018.

The hypotheses are:

1. Remote sensing serves as a valuable method for deriving high spatial resolution albedo, though over- or underestimations are supposed.

2. A distinct age-albedo pattern is predicted:

   2.1 In very young stands with low C sequestration, a high albedo is expected, since canopies are less dense in young stands. Because relative albedo changes (i.e., albedo change between initiation stage and young stands) are small in very young stands, the NEP might play a stronger role – leading to net positive radiative forcing of very young stands.

   2.2 For very old stand ages, the maximum positive albedo-induced radiative forcing is expected due to the highest relative albedo changes (i.e., albedo change between initiation stage and old stands) with maximum canopy closure. Since the C sequestration potential is reduced in very old stands (Peichl et al. 2023a), its relative contribution to the climate effect might be smaller, possibly resulting in a net radiative forcing might close to zero.

3. A generally high relative contribution of the albedo to the net climate effect due to a) the masking of snow in winter (Li et al. 2015), which could possibly influence the average annual albedo, and b) the generally low C storage rates in the boreal biome (Jackson et al. 2008).

4. Optimum net climate effects are expected in middle-aged stands where maximum C sequestration potential is reached, and the canopy is not fully closed yet – resulting in a strong influence of the C-flux induced negative radiative forcing.

Material and Methods

2.1 Study site

The study site is located in the Krycklan Catchment (KC) area (64°14′ N, 19°46′ E, 6780 ha) in Northern Sweden and belongs to the boreal biome (Laudon et al. 2021). The 30-year (from 1991-2020) mean annual precipitation is 638 ± 40 mm, the mean annual air temperature is 2.4 ± 0.3 °C, and the climate is cold, temperate, and humid. Elevations range from 138 m.a.s.l. (in the SE part) to 339 m.a.s.l. (in the NW). The lower part is dominated by sediment soils, whilst till-soils are found in the higher altitudes. Present land cover types are forests (87%), mires (9%), agricultural lands (2%), lakes (1%) and rock outcrops (1%). Scots pine (*Pinus sylvestris* L.) and Norway spruce (*Picea abies* (L.) H. Karst) dominate the forest (63% and 26%, respectively), and the stands are mixed with deciduous trees like *Betula* spp. *Alnus incana* (L.) Moench., and *Populus tremula* L. (11%). Ericaceous shrubs are present in the understory layer (e.g., *Vaccinium myrtillus* L*., Vaccinium vitis-idaea* L.) and moss mats (*Hylocomium splendens* (Hedw.) Br. Eur. and *Pleurozium screberi* (Brid) Mitt.). The forests are managed under rotation forestry, creating different stands of even age which are thinned and regenerated artificially. The stands are harvested via clear-cuts (excluded individual trees for retention).

In this study, 50 forests stands with different ages (i.e., years passed after establishment of stand) were selected. The stand age ranges from 5 to 211 years with five age classes: initiation (5 to 27 years old, $n = 8$), young (31 to 58 years old, $n = 9$), middle-aged (61 to 78 years old, $n = 13$), mature (80 to 105 years old, $n = 14$) and old (131 to 211 years old, $n = 6$). Each stand was categorized by the main tree species (pine, $n = 28$, and spruce, $n = 22$). The classification is rooted in a 350 m x 350 m grid covering 556 permanent plots of forest inventory (Martínez-García et al. 2022). A map of the KCS representing the landscape variations in aboveground biomass (AGB, Mg ha^{-1}), the 50 forest plots and their species composition as well as stand age is shown in Figure 2.
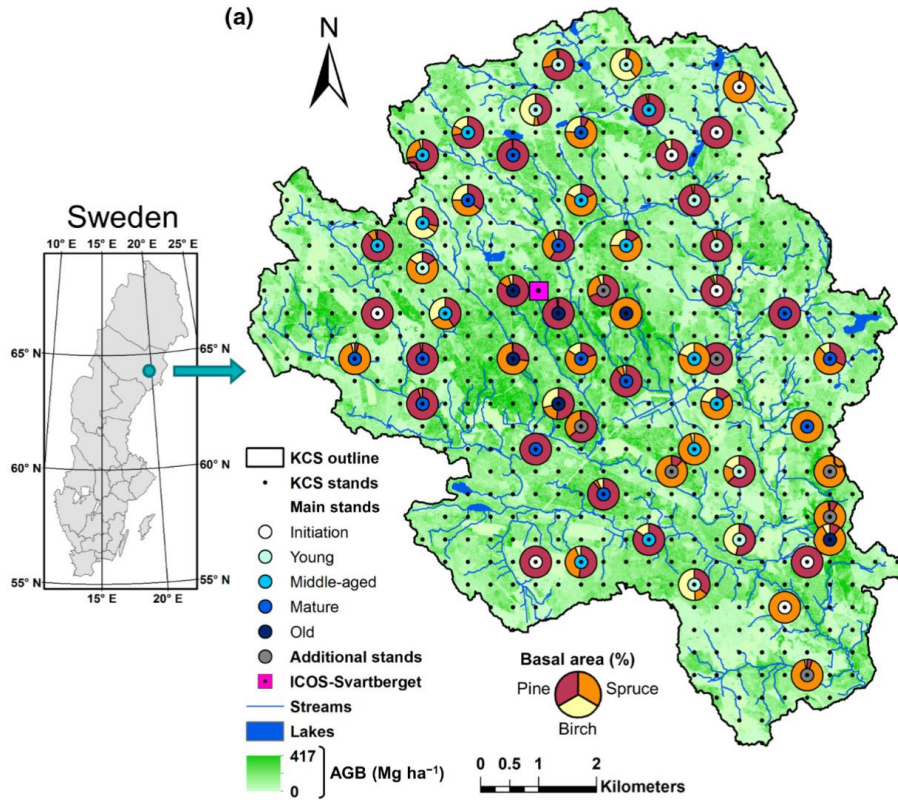
Figure 2.: Map of the Krycklan Catchment (KC) in Northern Sweden showing the variations in aboveground biomass data (AGB, Mg ha⁻¹), the 50 forest plots, their stand ages, and species composition. The map is taken from Peichl et al. (2023a),

2.2 Carbon flux measurement

Carbon balance data were available from Peichl et al. (2023a), these data included measurements of the C balance, defined as the net ecosystem production (NEP), over 3 years (2016-2018), combining chamber-based C flux measurements and forest inventory data. NEP was assessed as the combination of net primary production (NPP) and heterotrophic respiration (RH) including C fluxes and pools of trees, understory and soil, with

$$NEP = NPP - RH \qquad (1)$$

and positive NEP describing net C uptake and negative NEP net C emission. NPP was calculated by summing up tree and understory NPP (NPP_t and NPP_u, respectively, see equation 2), considering above ($ANPP_t$ and $ANPP_u$, see equation 3a) and belowground biomass ($BNPP_t$ and $BNPP_u$, see eq. 3b).

$$NPP = NPP_t + NPP_u \qquad (2)$$

$$NPP_t = ANPP_t + BNPP_t \qquad (3a)$$
$$NPP_u = ANPP_u + BNPP_u \qquad (3b)$$

NPP_t of aboveground and belowground biomass was measured via changes in C pools via litterfall and tree diameter at breast height on forest inventory plots and tree increment cores. NPP_u of aboveground and belowground biomass was estimated using destructive clipping of subplots and annual shoot length increments. Belowground fine roots were estimated using the ingrowth core method. RH was calculated as soil heterotrophic respiration (RH_s) and deadwood heterotrophic respiration (RH_{dw}, see equation 4).

$$RH = RH_s + RH_{dw} \qquad (4)$$

RH_s was estimated using chamber measurements of CO_2 fluxes on each plot. RH_{dw} was estimated by multiplying the above- and below-ground deadwood C pools with decomposition rate constants. For further details on methods for deriving the C balances, please refer to Peichl et al. (2023a). The dataset and the landscape variability of NEP are described in the following section 2.3.

Apart from NEP data, further stand data was available from the work of Peichl et al. (2023a) and used in this study to explain landscape variations in NEP, albedo and resulting radiative forcing. Those stand data included: NEP (g C m^{-2} yr^{-1}), age (yr), stand age class, dominant tree species, tree density, and Leaf Area Index (LAI, m^2 m^{-2}).

2.3 NEP dataset

Peichl et al. (unpublished data) used the plot-level NEP data and literature-based NEP data for respective landscape elements (forests, lakes, agricultural land, etc.) for scaling the C-balance to the whole Krycklan catchment. Figure 3 shows this upscaled map of the catchment-level NEP of the year 2016. The mean catchment NEP for the years 2016-2018 is 124.61 g C m^{-2} yr^{-1}. The upscaled NEP map was used in the present study to compute a catchment-level radiative forcing.
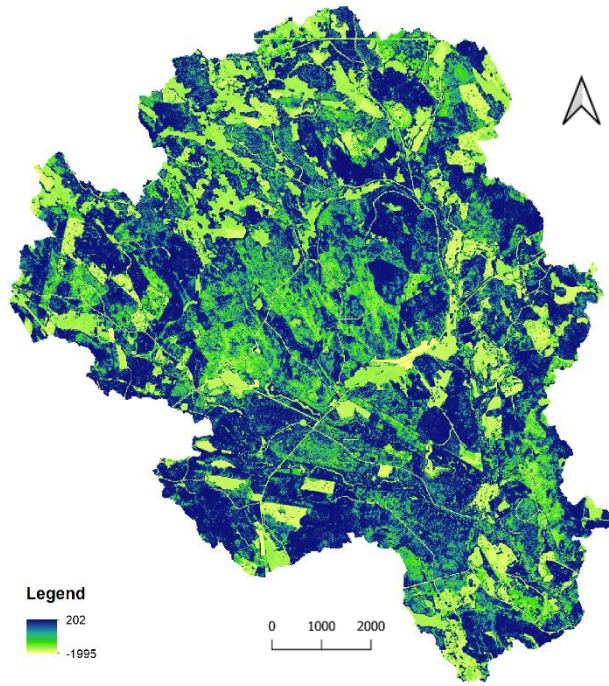
Figure 3.: Upscaled map of catchment-level Net Ecosystem Production (NEP, gC m⁻² yr⁻¹) of the year 2016 over the Krycklan Catchment (unpublished data).

Peichl et al. (2023a) also analysed the landscape variability of NEP amongst the 50 forest plots. Their analysis showed a distinct age-NEP pattern: net C emission was observed in the first stand years, followed by a sharp increase in NEP (and consequently a net C fixation) in the following decades with a peak in the mature age class and a gradual decline in older forests (Figure 4). Figure 4 shows the NEP-age dataset by Peichl et al. (2023a): the black dots are empirical NEP data whilst the red line represents a fitted NEP-age relationship (Peichl et al. 2023b). Additionally, mean and median NEP values per stand age class are shown in Table 1. More details of the age-NEP pattern are described in Peichl et al. (2023a).

Table 1.: Median and mean NEP (g C m⁻² yr⁻¹) values of the five stand age classes initiation (n=8), young (n=9), middle-aged (n=13), mature (n=14), old-growth (n=6), according to Peichl et al. (2023a).

stand age class	years	median NEP	mean NEP
1 – initiation	5-27	39.24	54.97
2 – young	31-58	126.49	140.14
3 – middle-aged	61-78	140.19	174.49
4 – mature	80-105	147.74	150.77
5 – old-growth	131-211	133.67	137.92

$$NEP = -488.18 + 308.77 \times \ln(age) - 37.3 \times [\ln(age)]^2$$
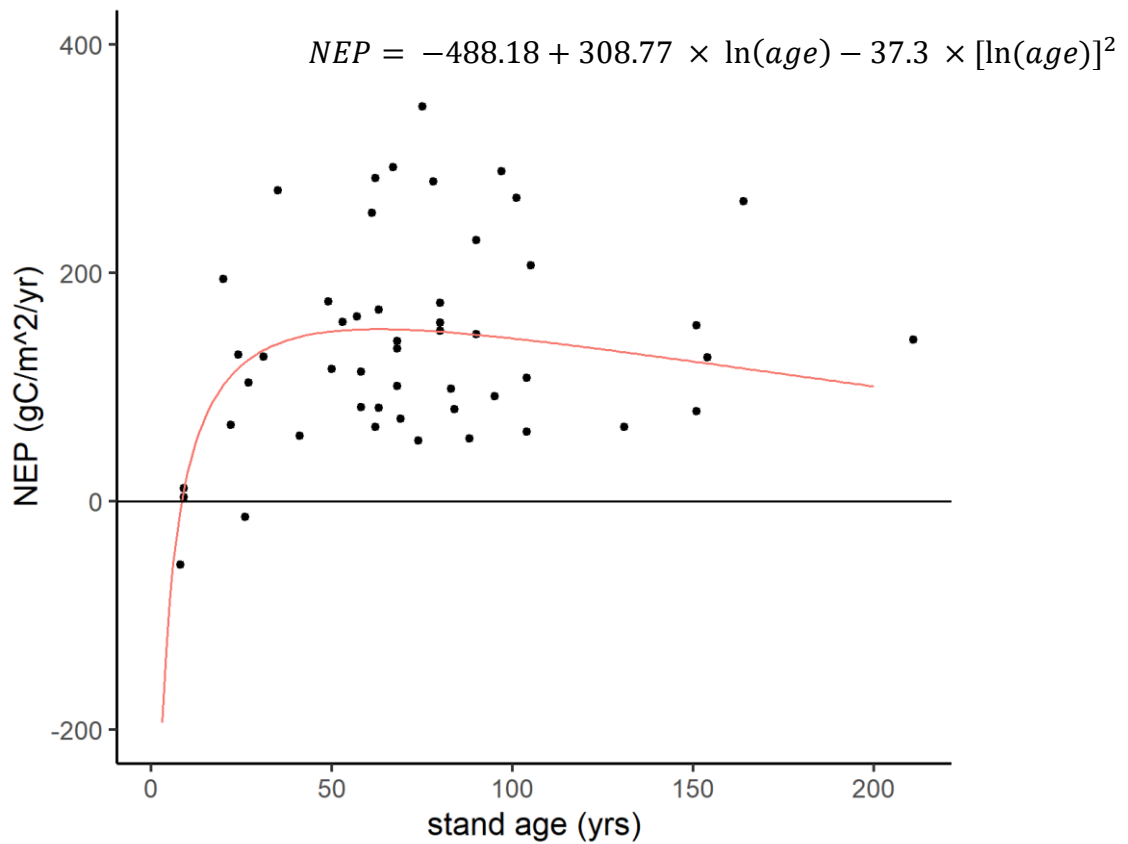
Figure 4.: Age-NEP relationship for the empirical NEP data (black dots) and the fitted NEP values (red line) with the NEP formula according to Peichl et al. (2023b).

These datasets (the upscaled albedo map and the plot-based NEP values) were used to calculate the C-flux driven radiative forcing of the Krycklan Catchment forest.

2.4 Datasets for validation of remotely sensed albedo data

To validate the remotely sensed albedo estimations they were a) aggregated from S2 to MODIS resolution and then compared with the available MODIS Black Sky Albedo product (MCD43A3.061 MODIS Albedo Daily 500 m), b) compared to tower-based ground measurements of albedo in clear-cut and old-growth stand reference sites inside and outside the Krycklan catchment, and c) compared with ground-based LAI measurements. The location of the clear-cut reference site is

64°10'37.344'' N, 19°51'52.171'' E. Half-hourly tower-based albedo measurements were available for this site for the year 2021. The mean full year albedo between the local hours 10-14 h was calculated and used as a reference albedo for clear-cut sites. The old-growth stand (Svartberget) is located in the Krycklan catchment (64°15'N, 19°46'E) and part of the Integrated Carbon Observation System (ICOS) National Network Sweden (https://www.icos-sweden.se/Svartberget, accessed 06/06/2023). A mean full year albedo was calculated for this site based on tower-based incoming and outgoing solar radiation data between 10 and 14 h local time (for 2019 for Svartberget and for 2021 for the clear-cut site). It was used as a reference albedo for old-growth stands and compared with mean remotely sensed albedo data for the Svartberget location.

2.5 Albedo retrieval

2.5.1 Algorithm theory

Surface albedo is the ratio between on the hemispherical incoming and outgoing radiation via surface reflectance. It changes temporally and spatially, depending on the surface structure and its dynamics (Li et al. 2018) as well as the sun angle. Calculating albedo requires several aspects: estimating the allocation of direct and diffuse incoming radiation, and merging surface reflectance over the hemispherical directions (Li et al. 2018). The anisotropic nature of natural land surfaces (Wanner et al. 1997) requires a description of that anisotropic light reflection. The bidirectional reflectance distribution function (BRDF) describes this reflection under varying solar and viewing angles (Nicodemus et al. 1977; Schaepman-Strub et al. 2006). Two extreme cases describe a) completely direct illumination conditions, called black-sky albedo (BSA), and b) completely diffuse illumination conditions (white-sky albedo, WSA, Lucht et al., 2000). The BSA is integrated over all viewing angles and the WSA is integrated over all illumination angles. The actual surface albedo A (also called Blue-Sky albedo) is somewhere in-between and can be calculated as a function of BSA and WSA, using an atmospheric optical depth as weighting (Lucht et al. 2000).

Whilst albedo and BRDF products exist, e.g., from the MODerate-resolution Imaging Spectroradiometer (MODIS), they lack on a finer spatial resolution (e.g., from Sentinel-2 at 10 m resolution). However, Shuai et al. (2011) propose an algorithm for deriving surface albedo at finer resolutions by coupling surface reflectance of near-nadir observing sensors like Sentinel-2 with MODIS BRDF products. This approach was validated for Landsat and Sentinel-2 products over different land cover types with a root-mean-square error of < 0.05 (Shuai et al. 2011; Li et al. 2018). The approach expects that the ratio between the albedo and

the near-nadir reflectance – also called AN ratio (a) – for the BSA and WSA are the same for MODIS as for Sentinel-2 (S2), when the same area observed (Li et al. 2018). This is described in equations 5a and 5b:

$$\bar{a}_{\lambda,S2}(\Omega_{S2}) \approx \bar{a}_{\lambda,m}(\Omega_{S2}) \text{ for the spectral BSA AN ratio} \qquad (5a)$$
$$\bar{\bar{a}}_{\lambda,S2}(\Omega_{S2}) \approx \bar{\bar{a}}_{\lambda,m}(\Omega_{S2}) \text{ for the spectral WSA AN ratio} \qquad (5b)$$

with $\bar{a}_{\lambda,S2}$ and $\bar{\bar{a}}_{\lambda,S2}$ describing the BSA and WSA spectral AN ratio, respectively. The subscript λ stands for the spectral band, whilst *S2* and *m* denote for S2 and MODIS pixels, respectively. Ω_{S2} refers to the S2 sun-view geometry and is represented by the solar zenith angle θ_s and the view zenith angle θ_v of the S2 image that was taken on the same day as the MODIS image over the same area.

Calculation of MODIS AN ratios
The MODIS AN ratios are calculated as:

$$\bar{a}_{\lambda,m}(\Omega_{S2}) = \frac{BSA_{\lambda,m}(\theta_s)}{R_{\lambda,m}(\Omega_{S2})} \qquad \text{for spectral MODIS BSA AN ratio} \qquad (6a)$$
$$\bar{\bar{a}}_{\lambda,m}(\Omega_{S2}) = \frac{WSA_{\lambda,m}}{R_{\lambda,m}(\Omega_{S2})} \qquad \text{for spectral MODIS WSA AN ratio} \qquad (6b)$$

where $BSA_{\lambda,m}(\theta_s)$ is the MODIS BSA for a given spectral band under the given solar zenith angle, $WSA_{\lambda,m}$ is the MODIS WSA for the given spectral band and $R_{\lambda,m}(\Omega_{S2})$ is the MODIS bidirectional reflectance at S2 sun-view geometry.

Calculation of MODIS bidirectional reflectance
$R_{\lambda,m}(\Omega_{S2})$ is defined as

$$R_{\lambda,m}(\Omega_{S2}) = f_{iso}(\lambda) + f_{vol}(\lambda)\, K_{vol}(\theta_s) + f_{geo}(\lambda)\, K_{geo}(\theta_s) \qquad (7)$$

with $f_{iso}(\lambda), f_{vol}(\lambda), f_{geo}(\lambda)$ being the isometric, volumetric and geometric weighting parameters provided in the MODIS BRDF product. K_{vol} and K_{geo} are the volumetric and geometric kernels and are dependent on the sun zenith angle (θ_s) and the view zenith angle (θ_v) and the relative sun-view azimuth angle (φ) (Roujean et al.,1992). The kernels represent the basic scattering types (volumetric and geometric scattering) of land surfaces (Lucht et al. 2000). The volumetric scattering kernel K_{vol} represents scattering effect caused by interleaf gaps in the canopy, whilst the geometric scattering kernel K_{geo} represents scattering effects caused by intercrown gaps (Lucht et al. 2000). The description of their calculation can be found in Lucht et al. (2000). For the present study, the calculation by Lucht

et al. was carried out with a modified height-to-base ratio of the trees (set to h/b = 1, see equation 41 Lucht et al. 2000), because the computation of the trigonometric function cos(t) (see equation 41 in Lucht et al. 2000) did otherwise not produce an output.

Calculation of MODIS BSA and WSA

The volumetric and geometric kernels K_{vol} and K_{geo} in equation 7 are difficult to solve analytically, and hence for the BSA and WSA they are often approximated using $h_{vol}(\theta_s)$ and $h_{geo}(\theta_s)$ as approximations for the BRDF (Lucht et al. 2000). These approximations are acceptable for view and sun zenith angles up to 80°. According to the look-up Tables by Lucht et al. (2000)

$$h_{vol}(\theta_s) = -0.007574 - 0.070987\theta_s{}^2 + 0.307588\theta_s{}^3 \qquad (8a)$$
$$h_{geo}(\theta_s) = -1.284909 - 0.166314\theta_s{}^2 + 0.041840\theta_s{}^3 \qquad (8b)$$

so that

$$BSA_{\lambda,m}(\theta_s) = f_{iso}(\lambda) + f_{vol}(\lambda)\, h_{vol}(\theta_s) + f_{geo}(\lambda)\, h_{geo}(\theta_s) \qquad (9)$$

Integrating the kernel approximations $h_{vol}(\theta_s)\, h_{geo}(\theta_s)$ and over the sun zenith angles θ_s gives the WSA integrals H_{iso}, H_{vol} and H_{geo}. According to Table 1 in Lucht et al. (2000)

$$H_{iso} = 1 \quad \text{and } H_{vol} = 0.189184 \text{ and } H_{geo} = -1.377622$$

Then, the WSA can be calculated as:

$$WSA_{\lambda,m} = f_{iso}(\lambda)H_{iso} + f_{vol}(\lambda)\, H_{vol} + f_{geo}(\lambda)\, H_{geo} \qquad (10)$$

Calculation of S2 BSA and WSA

From the AN ratio derived from the MODIS BSA and WSA (see equation 6a and 6b) the S2 BSA and WSA AN ratios can be inferred (see equation 5a and 5b) so that the S2 BSA and WSA can be calculated for each S2 pixel as

$$BSA_{\lambda,S2}(\theta_s) = \bar{a}_{\lambda,m}(\Omega_{S2})\, R_{\lambda,S2}(\Omega_{S2}) \quad \text{for the S2 BSA} \qquad (11a)$$
$$WSA_{\lambda,S2}(\theta_s) = \bar{\bar{a}}_{\lambda,m}(\Omega_{S2})\, R_{\lambda,S2}(\Omega_{S2}) \quad \text{for the S2 WSA} \qquad (11b)$$

with $R_{\lambda,S2}(\Omega_{S2})$ being the atmospherically corrected surface reflectance measured with the S2 sensor (Level 2A product).

Calculation of the S2 Blue Sky Albedo

From the BSA and WSA the actual spectral Blue-Sky albedo ($\alpha_{\lambda,S2}$) can be calculated as follows (Shuai et al. 2011):

$$\alpha_{\lambda,S2}(\theta_s) = \big(1 - \beta(\theta_s)\big)BSA_{\lambda,S2}(\theta_s) + \beta(\theta_s)WSA_{\lambda,S2}(\theta_s) \tag{12}$$

with $\beta(\theta_s)$ describing the weighting of direct and diffuse sunlight (Shuai et al. 2011), also called atmospheric optical depth (He et al. 2018), with 0.2 as a default value as described by He et al. (2018).

Narrow-to-broadband conversion

Further, a narrow-to-broadband conversion is applied to estimate the broadband albedo (A) from only a few narrow (spectral) bands, in the present study the VIS bands (Li et al. 2018; Liang & Wang 2020).

$$A = c_0 + \sum_{i=1}^{n} c_i \alpha_{\lambda_i,S2}(\theta_s) \tag{13}$$

where A denoted the broadband albedo, $\alpha_{\lambda,S2}(\theta_s)$ the spectral Blue-Sky albedo, and c_i ($i = 0, 1, \ldots, n$, with n being the number of spectral bands) are the band conversion coefficients. The visible spectrum (VIS) coefficients for S2 as published by Li et al. (2018) were used for this calculation, which cover the spectral range of $450 - 700$ nm (Table 2). For simplification purposes, only the snow-free VIS conversion coefficients were used.

Table 2. Narrow-to-broadband conversion coefficients c_i for S2 VIS bands for retrieving the broadband albedo (A), from Li et al. (2018).

	$c_{Band\,2}$	$c_{Band\,3}$	$c_{Band\,4}$	c_0
Snow-free VIS	0.5673	0.1407	0.2359	-0.0048

2.5.2 Datasets and data processing strategy

Datasets

For retrieving albedo values of the Krycklan Catchment, the Sentinel-2 MSI Level-2A reflectance product (S2 Level 2A) was combined with the MODIS MCD43A1 V6.1 BRDF-Albedo Model Parameters Daily 500 m. The S2 Level-2A product is a multi-spectral, high resolution, cloud-free Bottom of Atmosphere reflectance product, derived from two identical polar-orbiting satellites (Sentinel-2A and

Sentinel-2B) equipped with a multi-spectral instrument (ESA, 2015). Since the spectral response curve of S2A and S2B are similar (Lin et al. 2022), both satellite product were used in this study. The radiometric resolution of the S2 satellites is 12-bit with a radiometric error allowance of 5%, which makes the retrieval of surface signals viable (Sentinel-2 Team, 2021). The MCD43A1 product provides surface anisotropy information via the isometric, volumetric and geometric weighting parameters used in equation 4 (Lucht et al. 2000; Wang et al. 2018).

A 10 m pixel resolution were chosen for the albedo retrieval, since the corresponding C balance data have a plot resolution of 10 m. That way, albedo and corresponding C datasets could be combined accurately without losing information on the stands. For retrieving a 10 m albedo product the S2 bands B2 (448-546 nm), B3 (538-583 nm), and B4 (656-684 nm), were used, which correspond to the blue, green, red (RGB) – also summarized as visible (VIS) spectrum. For the MODIS products the equivalent bands within the same wavelength range were used, meaning B3 (459-479 nm), B4 (545-565 nm), and B1 (620-670 nm), respectively (Li et al., 2018, Table 3). In many studies the albedo is determined as the shortwave (SW) albedo, taking into account a wavelength spectrum of ca. 300 – 5000 nm (Li et al. 2018). In this study, a smaller wavelength range from ca. 450 – 700 nm (VIS) was used as an approximation for the full SW broadband spectrum. This is based on the observation that the most amount of solar irradiance ranges in this wavelength spectrum, whilst a smaller fraction is located in the adjacent wavelength ranges (Ranabhat et al. 2016). The same approach was used for the narrow-to-broadband conversion, where the conversion coefficients for the VIS spectrum were used.

Table 3. Corresponding band names and bandwidth (in nm) of the four bands from the S2 and MODIS, respectively, that were used for the 10 m resolution albedo retrieval.

Common band name	Blue	Green	Red
S2[a]	Band 2	Band 3	Band 4
	448-546	538-583	656-684
MODIS[b]	Band 3	Band 4	Band 1
	459-479	545-565	620-670

[a]https://sentinel.esa.int/web/sentinel/technical-guides/sentinel-2-msi/msi-instrument (accessed 27/03/2023), [b] https://modis.gsfc.nasa.gov/about/specifications.php (accessed 27/03/2023)

Data processing strategy

The data was downloaded for the area of interest using Google Earth Engine (GEE) for the period March 2017 to March 2019. S2 Level-2A data only existed from March 2017 on, even though the NEP data are from 2016-2018. The assumption here is that the changes of the relationship between albedo and C sequestration from one year to the other year with similar climatic conditions is negligible. Cloud-masking for retrieving S2 cloudless image was done via the *S2cloudless* algorithm

in Google Earth Engine (GEE Community, 2023) with filtering to a maximum image cloud cover of 20%. MODIS products were then downloaded for the same dates as S2 cloud-free images were available. Following the approach described in section 2.3.1 the albedo was retrieved in the following steps:

1. calculation of MODIS bidirectional reflectance at S2 sun-view angle (equation 7)
2. calculation of spectral MODIS BSA (equation 9) based on kernel approximations (equations 8a & 8b)
3. calculation of spectral MODIS WSA (equations 10)
4. inferring of S2 spectral BSA and WSA AN ratio (equations 5a & 5b) based on MODIS spectral BSA and WSA AN ratios (equations 6a & 6b)
5. calculation of S2 spectral BSA and WSA based on S2 AN ratios (equations 11a & 11b)
6. calculation of S2 Blue Sky Albedo (equation 12)
7. narrow-to-broadband conversion of spectral albedo to broadband albedo (equation 13)

A yearly mean value for the albedo was calculated for each pixel using the complete remotely sensed dataset of 2018-2019, resulting in one Blue Sky Broadband Albedo map of Krycklan. Blue Sky Broadband Albedo raster data was possible to compute between 2018/02/04 and 2018/11/03 as well as 2019/02/06 and 2019/11/05 (resulting in $n = 95$ remote sensing images), representing an estimation of the full-year albedo over Krycklan but missing albedo values for some winter months. Additionally, mean pixel values for the 10 m x 10 m forest plots were extracted from the full Blue Sky Albedo raster using zonal statistics in the *QGIS* software. These plot-level yearly means were used for further data analysis and the radiative forcing model. All calculations were carried out using *R* Version 4.2.3 (R Core Team, 2023) and the packages "raster" (Hijmans, 2023a), "GeoLight" (Lisovski and Hahn, 2013), "terra" (Hijmans, 2023b), "stringr" (Wickham, 2022) and "sp" (Pebesma and Bivand, 2005). All codes are made available on GitHub (see Appendix 1).

2.6 Radiative forcing models

2.6.1 C-flux RF

The C flux induced radiative forcing RF_C at any time t was calculated based on Frolking and Roulet (2007), where

$$RF_C(t) = \sum_{i=0}^{4}\left(RE\,f_i \times \int_0^t \phi_i(t')e^{\frac{t'-t}{\tau_i}}\,dt'\right) \qquad (14)$$

where RE is the radiative efficiency of CO_2 (0.0198×10^{-13} Wm^{-2} kg^{-1}), f_i is the fractional multiplier for the net flux into the reservoir (Table 4), $\phi_i(t')$ is the net flux of CO_2 to the atmosphere at time t' and τ_i is the residence time of gas in the reservoir i (Table 4). The RF model was used to calculate a yearly mean radiative forcing for each forest plot based on the respective C-flux data from 2016-2018.

Table 4.: CO_2 parameters for radiative forcing model based on Frolking and Roulet (2007).

Radiative efficiency (10^{-13} W m^{-2} kg^{-1})	Index	Fraction	Residence time τ_i (years)
0.0198	0	0.176	Infinite (modelled as 10^8 years)
0.0198	1	0.138	421
0.0198	2	0.186	70.6
0.0198	3	0.242	21.4
0.0198	4	0.259	3.42

2.6.2 Albedo-induced RF and total RF

The albedo-induced radiative forcing was calculated following the approach by Lohila et al. (2010):

$$RF_{glob} = RF_{loc} \times \left(\frac{S_{loc}}{S_{glob}}\right) \tag{15}$$

where RF_{glob} is the global radiative forcing caused by local radiative forcing RF_{loc}, scaled by the earth's surface with S_{loc} being the surface area of the plot and S_{glob} being earth's surface area (Lohila et al. 2010). Based on the estimated albedo values and annual mean shortwave downward radiation over Krycklan the amount of absorbed radiation was calculated. Annual mean shortwave downward radiation (SW_{in}) data for 2018 were taken from the National Aeronautics and Space Administration (NASA) Langley Research Center (LaRC) Prediction of Worldwide Energy Resource (POWER) Project funded through the NASA Earth Science/Applied Science Program (NASA, 2023). In line with Lohila et al. (2010), local radiative forcing of a plot was then computed as the differences in absorbed radiation between the youngest plot of the initiation age class ($SW_{abs,init}$) and the respective plot ($SW_{abs,plot}$), since the youngest plot is closest to a clear-cut reference albedo:

$$RF_{loc} = SW_{abs,plot} - SW_{abs,init} \tag{16}$$

$$SW_{abs,i} = SW_{in} - (SW_{in} \times \alpha_i) \tag{17}$$

Finally, the two datasets of albedo-induced RF and C-flux-induced RF were combined to a total RF (RF_{total}) for each plot:

$$RF_{total} = RF_{glob} + RF_c \qquad (18)$$

All codes for the radiative forcing model are made available on GitHub (see Appendix 1).

2.7 Statistical analysis

All analyses were conducted with yearly mean values, from 2016-2018 (for NEP) and from 2018-2019 (for albedo estimations) The estimated plot-level albedos were statistically analysed for significant correlations between stand data and albedo using nonparametric tests (Kendall's and Spearman's correlations). A principal component analysis (PCA) was performed to determine the explanatory factors for landscape variability of albedos. A mathematical fitting function was used to describe the age-albedo relationship: firstly, a linear model was calculated with the logarithmic-transformed age and the empirical albedo and RF data. Secondly, based on the linear model, fitted albedo data were calculated and plotted against the age together with the empirical albedoand RF data. Statistical analysis was carried out in R Version 4.2.3 (R Core Team, 2023) using "dplyr" (Wickam et al., 2023), "base" and "stats" (R Core Team, 2023) packages, and plots were created using "ggplot2" (Wickam, 2016).

Results

3.1 Remotely sensed albedo map

The estimations of the yearly mean albedos per pixel suggested that Blue Sky Broadband Albedo values over the catchment area varied between 0.009 and 0.408 with a mean of 0.131 and a median of 0.067 (Figure 5). Water bodies had the lowest albedo, whilst infrastructure elements (i.e., buildings and roads) were characterized by higher albedo values. The plot level albedo of the forest stands varied between 0.017 and 0.239, with a mean of 0.074 and a median of 0.058.
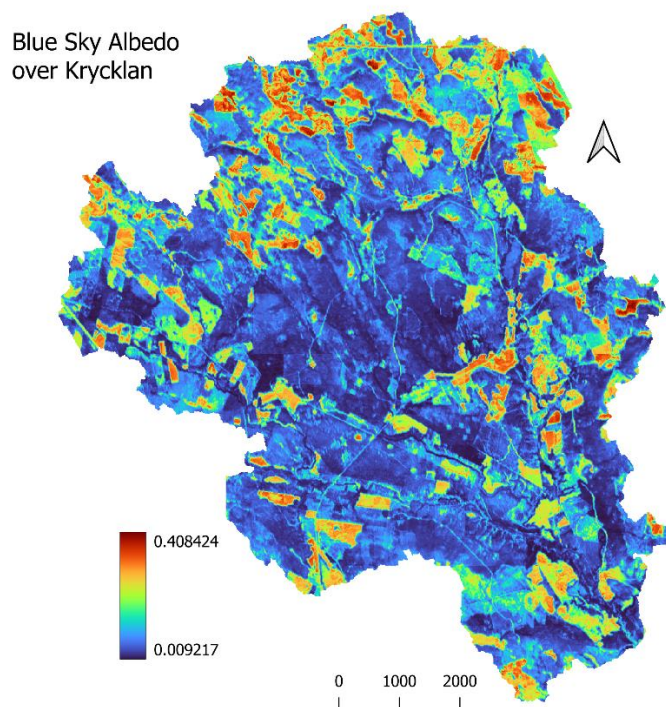
Figure 5.: Map of mean Blue-Sky Albedos over the Krycklan Catchment, estimated from data from the years 2018-2019. A high albedo translates to a high surface reflectance. Albedo values range from 0.009 and 0.408. The resolution is 10 m x 10 m and the scale bar unit is m.

3.2 Validation of remotely sensed albedo estimates

3.2.1 Aggregation to MODIS resolution

Since the used method of retrieving S2-resolution albedo estimations from MODIS BRDF is little explored, a validation of the dataset and the methodology is crucial. In this study, the S2 mean yearly Blue Sky Broadband Albedo was aggregated to a MODIS resolution and compared this with the 2018-2019 mean of the available MODIS Black Sky Albedo product. Compared to the S2 aggregated product, the MODIS product lacks the White Sky Albedo component but can still serve as a first benchmark for evaluating the albedo estimation. The differences between the MODIS product albedo values and the S2 aggregated albedo values ranged between 0.061 and 0.087 with no clear pattern for the different stand age classes, indicating an underestimation of albedo across all stand age classes. The aggregated albedo maps can be found in Appendix 3.

3.2.2 Comparison with reference sites

The two reference sites (Trollberget clear-cut and Svartberget mature forest) represent the starting and end points of a standard rotation period in boreal Sweden: an initiation phase, and a 110-year-old stand, respectively. Table 5 summarizes the comparison of the remotely sensed albedos over those stands and the tower-based measurements on the respective site. The comparison indicates an underestimation of albedo in the lower range values and an overestimation in the upper range values.

Table 5.: Comparison of remotely sensed Blue Sky Broadband Albedo estimations and tower-based albedo measurements over the two reference sites. The Trollberget clear-cut site is located outside the catchment, the Svartberget mature forest site is in the Krycklan catchment area.

site	remotely sensed albedo estimation	tower-based albedo measurement
Clear-cut	median A = 0.177	median A = 0.146
Svartberget (old-growth)	median A = 0.027	median A = 0.079

3.2.3 Comparison with ground-based measurements (LAI)

LAI and albedo of the plots correlate strongly (Spearman`s ρ = -0.742) and with high significance (p < 0.001). This is true across all stand age classes. The

relationship between albedo and LAI is as expected, since a higher LAI is usually associated with a thicker canopy, whilst a thicker canopy results in less reflectance and thus a lower albedo. The strength of the correlation reflects a reasonable dependency of the albedo on canopy thickness and thus confirms the robustness of the used albedo estimation methodology. The linear model between the log-transformed LAI and albedo shows a moderately good fit within the observed data range ($R^2 = 0.75$, with $p < 0.001$, Figure 6). A regression analysis shows a root-mean-square error (RMSE) of 0.029, indicating a moderately good fit between the predicted albedo values of the linear model and the empirical albedo data. The age-albedo relationship with the fitted albedo values from the linear model (black line in Figure 6) can be described for every x using the equation:

$$y = 0.139500 - 0.075252 \log(x) \qquad (19)$$

where y is the albedo and x is LAI ($m^2\,m^{-2}$). The mathematical fit describes an exponential decline of the albedo with higher LAI for Leaf Area Indices between ca. 1 and 6.
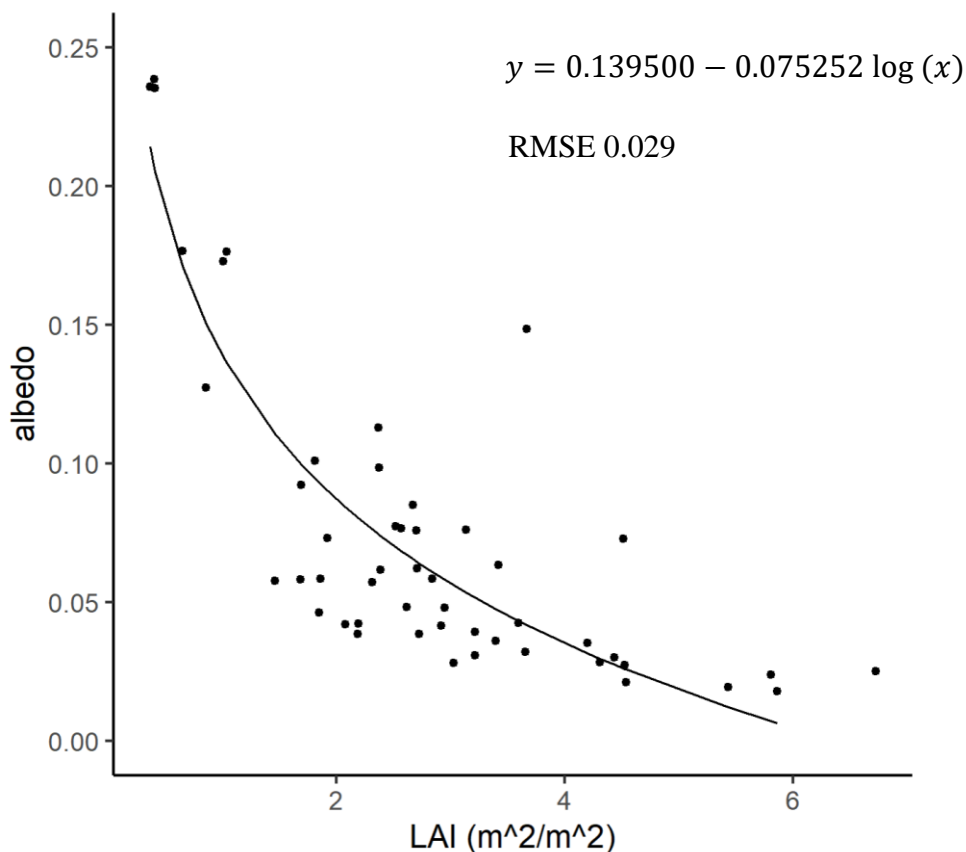
Figure 6.: Albedo-LAI (Leaf Area Index) relationship with empirical plot-level albedo data (black dots) and fitted albedo values from the linear model (black line). The linear model was calculated with the log-transformed LAI and the empirical albedo data. Residual standard error of model:

0.02922 on 48 degrees of freedom, $R^2 = 0.75$, with $p < 0.001$. Model estimates: Intercept 0.139500, log(x) -0.075252, with x being LAI ($m^2\ m^{-2}$), RMSE of regression: 0.029. The model outputs suggest a moderately good fit within the observed data range.

3.3 Drivers of landscape variability in albedo

Results from the PCA based on the 50 forest stands suggests that LAI, age, and stand age class were most strongly associated with albedo, since the respective arrows closely match with the PC1 axis which is strongly explained by albedo (points in the same direction, Figure 7). This is supported by the strength and significance of the correlations between albedo and those parameters. In contrast, the correlations of albedo with tree density, dominant tree species or NEP were weak. The PCA suggests a negative correlation between albedo and LAI as well as albedo and age since the respective arrows point in opposite directions. The two first Principal Components PC1 and PC2 explain 62% of the data variance.
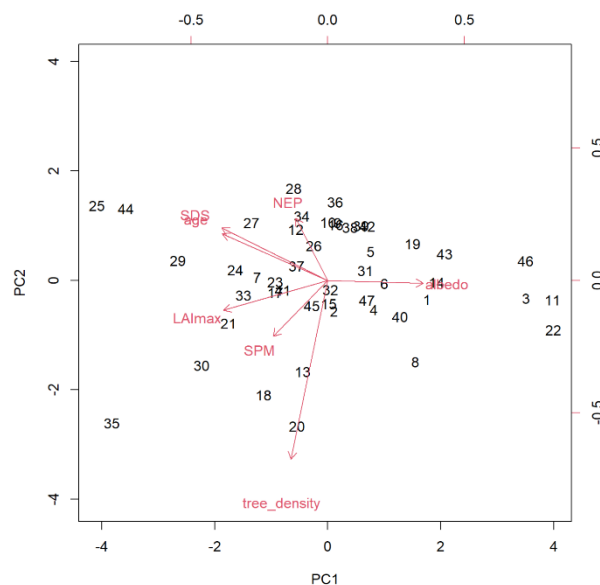
Figure 7.: Principal Component Analysis (PCA) loading plots of stand data on albedo across the studied forest landscape. Input parameters were age (yr), stand age class (SDS), dominant tree species (SPM, pine or spruce), tree density, Net Ecosystem Production (NEP, g C m^{-2} yr^{-1}), and leaf area index at peak growing season (LAImax, m^2 m^{-2}); n = 50 forest stands.

All available stand properties (age, stand age class, dominant tree species, tree density, NEP, LAI) were tested for correlations with plot-level albedo values. Highly significant correlations ($p < 0.001$) with albedo are present for age, stand

age class, and LAI; significant correlations ($p < 0.05$) for tree density. Age and albedo are correlated negatively (Kendall´s τ = -0.512), the same applies to stand age classes and albedo (Kendall´s τ = -0.505). The strongest correlation is detected between albedo and LAI (Spearman´s ρ = -0.742) whilst tree density shows a slight negative correlation with albedo (Kendall´s τ = -0.208). Results of the tested correlations are summarized in Table 6.

Table 6.: Relationships between broadband albedo (A) and various stand properties, their significance levels and correlation coefficients using Kendal or Spearman correlation, respectively.

significance level	tested relationship	correlation coefficient
$p < 0.001$	A ~ age	Kendall´s τ = -0.512
	A ~ stand age class	Kendall´s τ = -0.505
	A ~ LAI	Spearman´s ρ = -0.742
$p < 0.05$	A ~ tree density	Kendall´s τ = -0.208
p not significant	A ~ dominant tree species	/

The age-albedo relationship is illustrated in Figure 8, 9 and Table 7 which show albedo values of the 50 forest plots grouped by the stand age classes. Table 7 summarizes the mean albedo values for each stand age class. The initiation stand age class shows the highest albedo values (mean albedo 0.178) which gradually decreases in the following stand age classes. The pattern shows a sharp decrease in albedo after the initiation stage to the young class (mean albedo 0.069) and a gradual slow decline in albedo from middle-aged (mean albedo 0.057) to mature (mean albedo 0.051) and old-growth stands (mean albedo 0.034) where the minimum albedo of 0.017 can be observed (Figure 8). The variance (Whiskers in Figure 8) of albedo is the maximal in the initiation age class and the lowest in the old-growth age class.
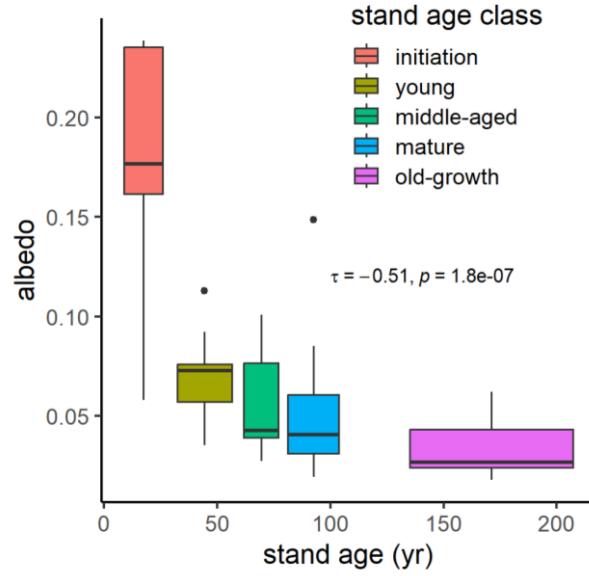
Figure 8.: Box-Whisker plot showing the age-albedo relationship grouped by stand age classes (initiation, young, middle-aged, mature, and old-growth) with Kendall correlation statistics (τ = -0.51, p < 0.001) of plot-level yearly mean albedo values of the forest plots (n = 50) in the Krycklan Catchment. Black bars in the boxes represent the stand age medians, Whiskers indicate the variance.

Table 7.: Median and mean albedo values of the five stand age classes initiation (n=8), young (n=9), middle-aged (n=13), mature (n=14), old-growth (n=6).

stand age class	age (years)	median albedo	mean albedo
1 – initiation	5-27	0.177	0.178
2 – young	31-58	0.073	0.069
3 – middle-aged	61-78	0.043	0.057
4 – mature	80-105	0.040	0.051
5 – old-growth	131-211	0.027	0.034

The linear model between the log-transformed age and log-transformed albedo shows a moderately good fit within the observed data range ($R^2 = 0.59$, with $p < 0.001$, Figure 9). A regression analysis shows a root-mean-square error (RMSE) of 0.030, indicating a moderately good fit between the predicted albedo values of the linear model and the empirical albedo data. The age-albedo relationship with the fitted albedo values from the linear model (black line in Figure 9) can be described for every x using the equation:

$$y = 1.151 \times x^{-0.726} \tag{20}$$

where y is the albedo and x is the stand age (years). The mathematical fit describes an exponential decline of the albedo with higher stand age for ages between ca. 5 and 165 years.

$$y = 1.151 \times x^{-0.726}$$

RMSE 0.030
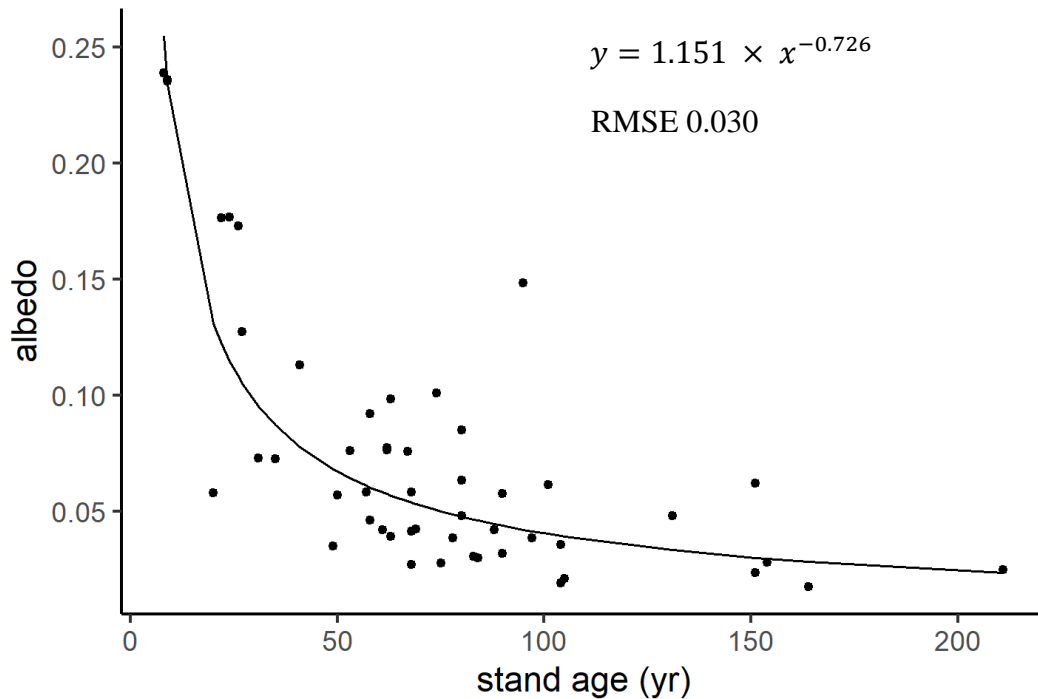
Figure 9.: Age-albedo-relationship with empirical plot-level albedo data (black dots) and fitted albedo values from the linear model (black line). The linear model was calculated with the log-transformed age and the empirical albedo data. Residual standard error of model: 0.434 on 48 degrees of freedom, R^2 = 0.59, with p < 0.001. Modelled relationship can be described as y = 1.151 × $x^{-0.726}$ with x being stand age (years) and y being albedo, RMSE of regression: 0.030. The model outputs suggest a moderately good fit within the observed data range. The compliance of the model-predicted and the reference values can be found in Appendix 4.

3.4 Radiative forcing of boreal rotation-forestry

3.4.1 C-flux induced radiative forcing

The resulting patterns in radiative forcing are – complementary to the C-flux vs. albedo patterns – contrary to each other (Figure 11a). Whilst C-flux leads to a positive radiative forcing (up to +0.446 nW m^{-2} yr^{-1}) for some stands in the initiation phase, all other stand age classes show a negative radiative forcing. Amongst the 50 forest plots, the RF varied between +0.446 and -2.769 nW m^{-2} yr^{-1}. The median RF of the initiation stage is -0.314 nW m^{-2} yr^{-1}, -1.013 nW m^{-2} yr^{-1} for the young

one, -1.123 nW m^{-2} yr^{-1} for the middle-aged, -1.184 nW m^{-2} yr^{-1} for mature stages and -1.071 nW m^{-2} yr^{-1} for old-growth stands. Figure 10 shows a loess smoothing of the dataset and displays the sharp decrease in radiative forcing after the initiation stage, a minimum in the middle-aged class and a stabilization thereafter. This pattern is complementary to the NEP-age pattern – e.g., the NEP peak in the middle-aged class (see Figure 4) translates to the minimum RF in the same age class (see Figure 10). Based on the upscaled NEP map (Figure 3) the catchment-level NEP-induced RF is -0.998 nW m^{-2} yr^{-1}.
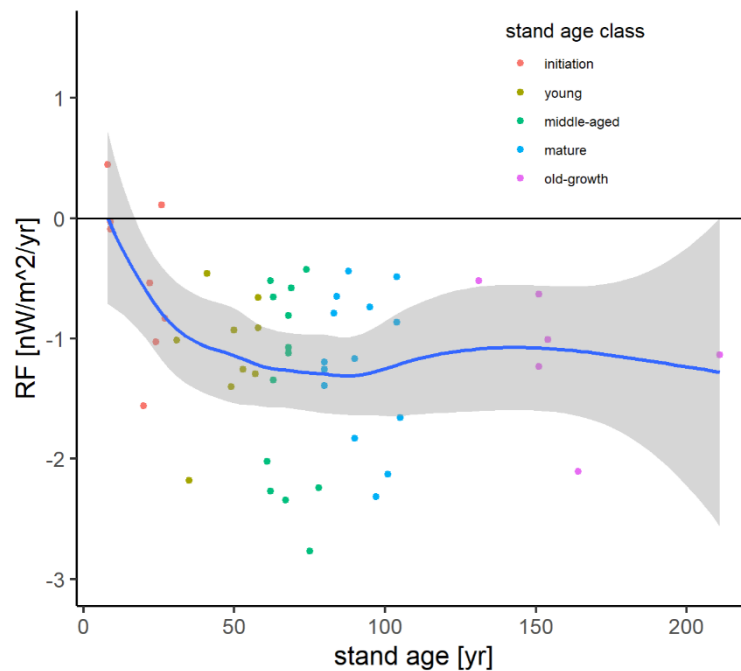
Figure 10.: C-flux induced radiative forcing based on the annual NEP values of the 50 forest plots, grouped by stand age classes. A loess smoothing is applied to the dataset (blue line, 95% confidence interval in grey) and shows a sharp decline in radiative forcing after the first decades and a minimum in the mature stand age class.

3.4.2 Albedo-induced radiative forcing

Contrary, the albedo-induced RF is always positive and ranges between 33.8 and 22654.7 W m^{-2} yr^{-1} for the local RF effect and between 0.0006 and 0.4442 nW m^{-2} yr^{-1} on a global scale, though the age patters are comparable for both local and global albedo RF and only differ in their magnitude (W m^{-2} yr^{-1} vs. nW m^{-2} yr^{-1}). For better comparison, only the global RF impact is presented here – the local RF effect is shown in Appendix 2. Global RF impacts of the 50 forest plots show a distinct pattern according to their age and stand age class (Figure 11a). The smoothing function (line in Figure 11a) shows a sharp increase in RF in the initiation age class up until the young class, followed by a slow and steady increase

in RF that converges towards a maximum RF of ca. 0.44 nW m^{-2} yr^{-1} in the oldest stand age class. Based on the catchment-level albedo map (Figure 5) the catchment-level albedo-induced RF is 0.217 nW m^{-2} yr^{-1}.

The linear model between the log-transformed age and RF shows a moderately good fit within the observed data range (R^2 = 0.68, with p < 0.001, Figure 11). A regression analysis shows a root-mean-square error (RMSE) of 0.065 nWm^{-2} yr^{-1}, indicating a moderately good fit between the predicted albedo values of the linear model and the empirical albedo data. The age-RF relationship with the fitted RF values from the linear model (black line in Figure 11b) can be described for every x using the equation:

$$y = -0.2125 + 0.1324 \log(x) \tag{19}$$

where y is the RF (nWm^{-2} yr^{-1}), and x is age (years). The mathematical fit describes an exponential increase of the RF with higher ages for stand ages between 5 and 200 years.
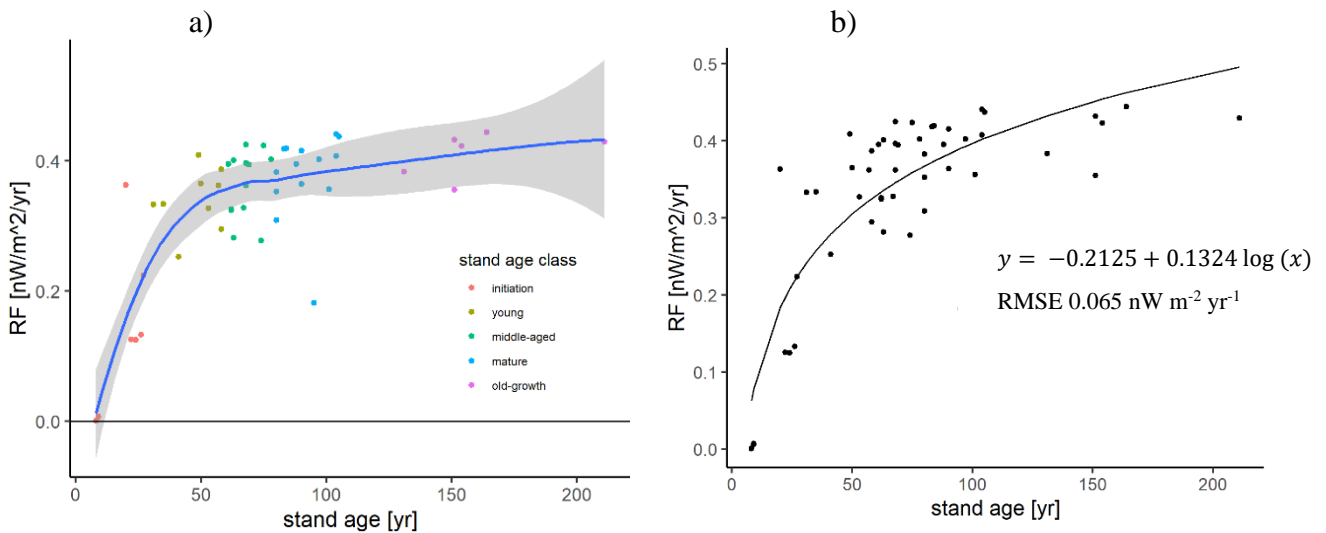
Figure 11.: Albedo-induced global radiative forcing, based on the relative albedo differences between the initiation stage and the respective forest plot. a) The data is grouped by stand age classes (initiation, young, middle-aged, mature and old-growth) and smoothed using the loess-function (blue line) with 95% confidence interval (grey). The pattern shows a sharp increase in radiative forcing during the initiation stage up until the young stage, followed by a convergence towards a maximum RF. b) relationship with empirical plot-level albedo data (black dots) and fitted albedo values from the linear model (black line). The linear model was calculated with the log-transformed age and the empirical albedo data. R^2 = 0.67 on 48 degrees of freedom, , with p < 0.001. Model estimates: Intercept 10.2125, log(x) 0.1324, with x being stand age (years), RMSE of regression: 0.065 nW m^{-2} yr^{-1}. The model outputs suggest a moderately good fit within the observed data range.

3.4.3 Net climate effect of KC forest plots and catchment

Combining the two components albedo and C-flux into a total radiative forcing model shows the higher magnitude – by factor three – of C-flux induced RF component compared to albedo-induced RF component (Figure 12a). Consequently, C-sequestration effects overpower albedo effects and result in a total climate effect that is like the C-induced climate effect alone (Figure 10 and 12b). Also, the albedo-induced RF shows a lower variance in data compared to the variance of C-induced RF, indicated by the respective 95%-confidence intervals (in grey, Figure 12a). Some plots in the mature age class (blue group, Figure 12b) are close to a net-zero climate effect when combining both albedo and C-sequestration, whilst the first years of the initiation stage still show a net positive RF. All the following age classes have a net negative RF effect.
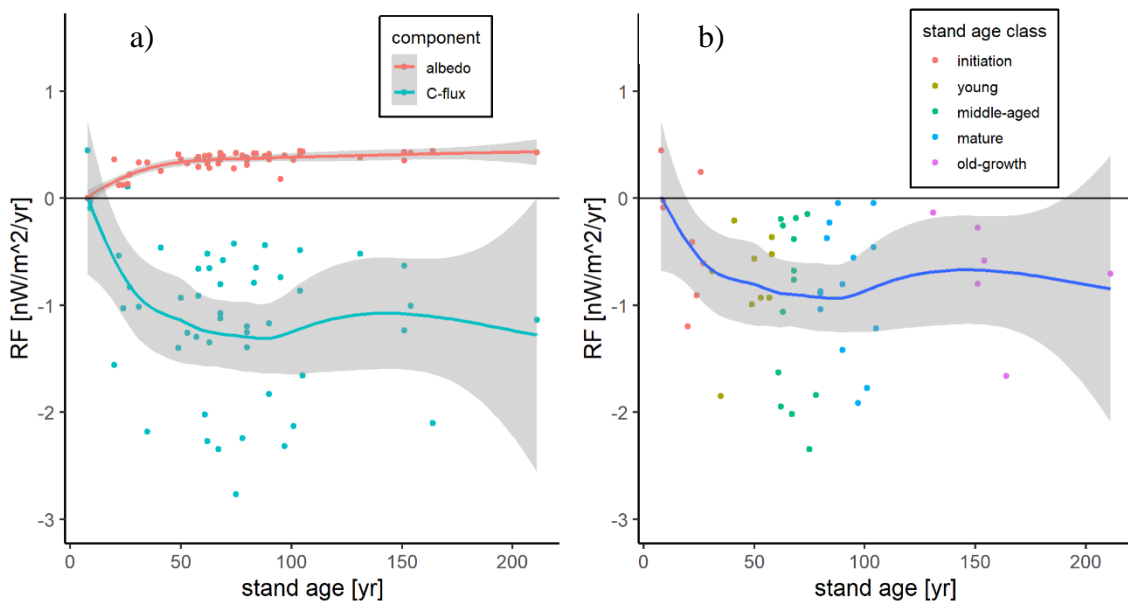
Figure 12.: a): Comparison of albedo-induced radiative forcing (orange line) and C-flux induced RF (blue line). The former component is characterized by a clearly lower magnitude compared to the latter component. The albedo-induced RF shows a lower variance in data compared to the variance of C-induced RF (see respective 95% confidence intervals in grey). b): Combined RF effects from the component's albedo and C-flux, grouped by stand age classes. The pattern in comparable to the C-flux induced RF alone since the magnitude of the NEP impact overpowers the albedo impact.

The shares in net radiative forcing of the albedo and NEP components – grouped by stand age class – are shown in Figure 13. In the youngest stand age class, the albedo contributes the least to the RF (18,90%) whilst the share of NEP-induced

RF is the highest in this age class (81,10%). For all the other stand age classes, the share of albedo-induced RF in the total RF is ca. 25% whilst the share of NEP-induced RF in the total RF is ca. 75%. Across all stand age classes, the albedo contributes to 25.25% and the NEP to 74.75% of the total RF (Figure 13).

The net catchment-level climate effect of the Krycklan catchment is -0.782 nW m^{-2} yr^{-1}. Based on the catchment-level forcings induced by albedo and C-dynamics, the RF for the whole KC is -0.782 nW m^{-2} yr^{-1}. Scaled to the catchment area (6780 ha) this results in a yearly RF of -0.053 W m^{-2} yr^{-1}.
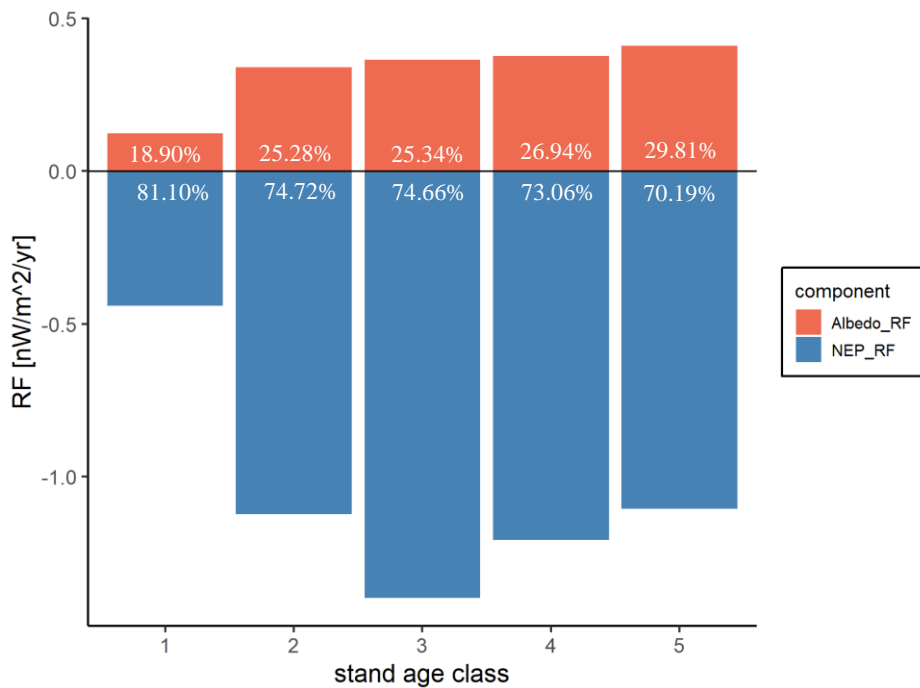
Figure 13: Relative contribution of the albedo component (red bars) and NEP component (blue bars) to the net RF (red and blue bars combined), grouped by stand age classes (1 = initiation, 2 = young, 3 = middle-aged, 4 = mature, 5 = old-growth). The numbers in the bars indicate the proportion (in %) of the summed up gross radiative forcing values.

Discussion

4.1 Remote Sensing as a tool for estimating albedo

The computed albedo values were in a reasonable data range of [0.009; 0.408] and thus are within the possible values of albedo ([0; 1]). A comparison of the remotely sensed albedo data with the reference sites shows a slight bias in the produced data. Compared to the reference sites, the albedo seems to be slightly overestimated in the upper range (initiation stage) and underestimated in the lower range (old-growth stage), indicating a regression towards the mean. The comparison with the MODIS product underlines the possible underestimation of albedo values.

Halim et al. (2019) report summer albedos of ca. 0.1 in old forest stands and higher winter albedos. This suggests an underestimation from the data in this study, though it could also result from missing albedo values in the winter months. In comparison, Kuusinen et al. (2014) report summer and spring albedo values between 0.02 and 0.06, which comply well with the range of albedo in this study. However, comparing the albedo data produced in this study with previously reported albedos is challenging since estimations and measurements take different seasons (seasonal or full-year albedo) into account. The used method can be seen as a valuable approach to derive small-scale albedo values via remote sensing, though more research is necessary to validate the approach. Also, more research is needed to test other inputs for the modified height-to-base ratio values (section 2.5.1) and detect ways of computing the Kernels with those values.

4.2 Interpretation of RF from carbon dynamics

Based on the available C-flux data, some of the youngest stands in the initiation phase showed a climate warming effect (i.e., positive RF) whilst a climate cooling (i.e., negative RF) was present along all other stand ages. This trajectory follows observed patterns in C-flux induced radiative forcing in other studies observing different forest management types (O'Halloran et al. 2012; Cherubini et al. 2018).

It also follows the expected successional change and unimodal curve that represents the successional NEP pattern (Peichl et al. 2023a).

Local underlying biogeochemical processes explain the successional pattern: after clear-cutting, organic matter decays at high rates, leading RH to exceed NPP of young trees. With ongoing succession, organic matter is decomposed – slowing down RH – whilst NPP of ageing trees increases, creating a carbon sink and thus a negative RF (Cherubini et al. 2018). Globally, the time lag between the release of C after a clear-cut and the removal fluxes leads to a short-term increase of atmospheric CO2 and thus a short-term climate warming (O'Halloran et al. 2012; Cherubini et al. 2018). In retention forestry of Swedish boreal pine forests, the RF changed from positive to negative already after ca. 15 years (Cherubini et al. 2018). In the present study, this point is reached earlier, after ca. 10 years. This challenges the notion of young stands under rotational forestry being climate warming and can be explained with relatively low heterotrophic respiration in the catchment (Peichl et al. 2023a), which usually contributes strongly to RF of C fluxes of young forest stands.

4.3 Stand age as a proxy for albedo and albedo-induced RF in rotation forestry

Variability of albedo values in the catchment area could be well explained by the stand age and stand age classes. The pattern shows an exponential decline of albedo in the first decades and a stabilization thereafter. The moderate R^2 of the fitted age-albedo relationship (Figure 9) underlines the exponential characteristics of the relationship between age and albedo. This supports hypotheses 2.1 and 2.2 which suggested maximum albedo values for young stands and minimum values for the oldest stands.

The pattern also complies with general age-albedo patterns in boreal forests previously reported by Halim et al. (2019) and Kuusinen et al. (2014). Their studies showed a rapid decline, especially of the VIS-based albedo and stabilization ca. 50 years after disturbance, similar patterns were reported by Cherubini et al. (2018) for retention forestry in Swedish boreal pine forests. However, albedo stabilization depends on the chosen reference scenario – in the case of referring the albedo change to a clear-cut (in the present study) the stabilization is naturally later than when referring the albedo change to a thinned forest. In the present study, stabilization starts at the age of ca. 100 years, suggesting a later stabilization, possibly due to a differing reference albedo scenario. The findings of this study comply with the impact an albedo-change due to natural disturbances had in a Canadian study by O'Halloran et al. (2012).

Within the age-albedo pattern, the aspect of age can be seen as a proxy for more complex successional changes – e.g., canopy structure – which develop with age (Halim et al. 2019). One of those successional changes that explain the distinct age-albedo relationship is the process of gradual regrowth of trees and progressive canopy closure (Cherubini et al. 2018). A clear-cut or initiation stage is characterized by a low LAI and higher amount of broadleaved understory (Amiro et al. 2006; Kuusinen et al. 2014), causing a higher albedo. Whilst the canopy closes over time, it reflects less due to the coniferous leaf structure and a higher LAI. In this study, the lowest albedo and albedo stabilization at around 0.03 is reached after ca. 100 years, indicating a maximum canopy closure at this stand age. This observation complies with a study by Bright et al. (2015) who observed albedo changes due to forest disturbances to be persistent until the canopy closes again. Generally, succession is considered to be slower in the boreal biome so that albedo changes lean towards a longer-lasting impact (O'Halloran et al. 2012). In the present results, the albedo begins to stabilize from ca. 100 years onward. However, a more detailed analysis of older stands would be necessary for determining the minimum albedo and with that age of full canopy closure with higher certainty.

Other studies of the boreal biome suggest a species-dependency on the age-albedo relationship: a stronger relationship was observed for spruce than for pine, mainly due to differing understory (Kuusinen et al. 2014). No such pattern could be observed in this study, since the dominant tree species showed no significance in explaining the albedo or the age-albedo relationship.

Since albedo changes are local and influence the local temperature, one could infer a continuous local cooling. However, this does not take changes in sensible and latent heat fluxes after clear-cutting into account and thus not always applies (Landry et al. 2016). Based on the age-albedo pattern, a climate warming (i.e., positive RF) could be observed across all stand ages since a clear-cut was chosen as the reference scenario for the relative albedo change in the RF model. Analogue to the age-albedo pattern, the age-RF pattern induced by albedo changes shows an exponentially increasing warming effect until the middle-aged stand class and only a gradual, slow increase thereafter. This indicates a maximum climate cooling which can be induced by albedo changes: cooling is limited by reaching the minimum reflectance due to a fully closed canopy during the successional process.

4.4 Relative importance of albedo and NEP in RF effects of boreal forests

Generally, RF of albedo effects observed in this study counter those of C sequestration (Figure 12), which complies with other studies (Bonan 2008;

Anderson et al. 2011; Mykleby et al. 2017). However, the magnitude of climate warming is offset by the magnitude of climate cooling effects caused by C-sequestration – which is nearly three times higher – for all stand age classes. The relative importance of NEP is the highest in the initiation stage (81,10%), which supports parts of hypothesis 2.1 which states that NEP might play a bigger role in very young stands.

The initiation stage is the only stand age class with a positive net RF, thus a net warming climate effect, though the general RF pattern follows the C-flux induced RF rather than the albedo-induced RF. Consequently, C-sequestration (responsible for ca. 75% of the net RF) overrules albedo (responsible for ca. 25% of the net RF) regarding the net climate effect – which contradicts hypothesis 3 as well as parts of hypothesis 2.2. This is true not only for the forest plots, but also for the entire catchment – consequently, the Krycklan catchment can be seen as a climate-cooling landscape element (-0.053 W m-2 yr-1). Possible explanations for the divergent pattern are explored further down.

Generally, the relative contribution of C-flux and albedo to the climate effect is highly uncertain so that the present results are supported by some studies and opposed by others (Bright et al., 2011; Cherubini et al., 2018; Kalliokoski et al., 2020; Kellomäki et al., 2021; Landry et al., 2016; O'Halloran et al., 2012). In line with the present results, Cherubini et al. (2018) reports a long-term net cooling due to strong C sink contributions in retention forestry of a Swedish pine forest, Lohila et al. (2010) observed the same pattern especially for nutrient-rich boreal forests. The management and the nutrient availability on the site could be one explanation for the dominance of C-sequestration – a high nutrient availability results in a high NEP, which reduced the relative contribution of albedo-induced RF.

The present results challenge other studies which observed a similar magnitude of albedo and C effects, leading to a net-zero climate impact (O'Halloran et al., 2012; Kellomaki et al., 2023). However, those study natural disturbances and thus might not be comparable with clear-cuts in rotation forestry. E.g., a beetle outbreak is less complete and discrete than a clear-cut, and a fire darkens the surface due to burning. This creates highly different disturbances than the clear-cuts in the present study.

Generally, the different observations show that patterns highly depend on the reference and underground albedo and the extent of snow coverage (Thompson et al. 2009; O'Halloran et al. 2012). It is also noteworthy that missing data in the winter months in this study – missing a crucial period and thus reducing the relative importance of albedo. The snow-masking effect of forest stands during snow periods is not fully accounted for due to lack of albedo data between mid-November and February.

In the future, the relative importance of albedo in the boreal zone will possibly change. When winters become milder and snow presence reduces, the snow-

masking effect of older stand ages will be less present and thus reduce the relative importance of albedo in the boreal zone. Overall, the present results underline an unclear picture about the relative importance of albedo vs C dynamics in climate effects of boreal forests. This stresses observations about C and albedo not necessarily being coupled during succession but rather following a highly complex process (O'Halloran et al. 2012).

The results indicate maximum radiative climate benefits (i.e., highest negative RF and thus highest cooling effect) in the middle-aged and mature stands, which confirms hypothesis 4. This might be due to a) maximum C sequestration potential in those stand age classes (Peichl et al., 2023a) and b) a not fully closed canopy. Those two factors combine the maximum negative RF of the C dynamics and a not yet fully exhausted positive RF potential due to albedo dynamics. According to the trajectory in Figure 12b, maximum climate cooling is reached for ca. 100-year-old stands. Comparing this result with the optimum rotation period based solely on the cumulative and current C-cycle (138 years, Peichl et al., 2023a) possibly points towards a lower optimum rotation period when including the albedo, though more research would be needed to support this with the present data.

4.5   Possible sources of errors and limitations of the study

Several possible sources of errors emerge from the used method. The highest amount of error sources lies in the albedo estimation. Thus, the estimated values come with high uncertainties. The BRDF used for computing the surface reflection can only be estimated and not measured, thus always producing a systematic error. Other systematic errors emerge from the band conversions, since MODIS and S2 bands differ slightly in their wavelengths. Missing data due to cloud-shadowing and high sun zenith angles produced missing albedo values in the winter months – leaving out a crucial period and thus producing an error in the full-year albedo estimation. Moreover, the modified height-to-base ratio (h/b) value might produce an error in the values of the Kernels. The timeframe of the present work did not allow for a further investigation of alternatives to compute the Kernels using other possible h/b values, so more research would be necessary. Since the S2 Level 2A product was not available before 2017/03 the period between 2017 and 2019 was chosen for albedo calculation instead of the years 2016-2018 (years for which C balances were calculated). Here, the assumption is that the albedo-C-flux-ration changes are negligible within one year, thus only creating a small error.

The timeframe and scope of the present work poses several limitations to the study. Firstly, MODIS pixels were not checked for homogeneity of land cover, though it is assumed because the Krycklan catchment is mostly covered by boreal

forests with little amounts of other land cover classes. Secondly, using the quality control layer of the MODIS BRDF product could be useful for future studies. Thirdly, no accuracy assessment of the computed albedo was performed, e.g., a comparison with more field measurements, since this would have exceeded the scope of this work. Nevertheless, a more elaborated validation would benefit future studies. Moreover, more investigations would have been necessary to choose a more robust reference albedo. No remotely sensed albedo data of a fresh clear-cut were available, instead the albedo of the youngest stand was used. Further analysis of clear-cut albedos over Krycklan could possibly yield a more robust result of albedo differences between stand ages. Lastly, a more thorough analysis of the produced data could produce a trajectory of radiative forcing along forest succession over time. A more elaborated RF model that takes longer time frame and a dynamic CO_2 background concentration into account could be one further step of analysis.

Conclusions

This study aimed to explore net climate effects of an understudied boreal alrea in Northern Sweden and discover the landscape variations of albedo in the forest landscape and the relative importance of C sequestration vs. albedo in the net climate effect of managed boreal forests under rotational forestry. Further, this study explored remote sensing as a tool for estimating albedo over those forests.

Overall, this study shows the potentials of using remote sensing for estimating albedo over boreal forests. The used method demonstrates a valuable starting point for deriving high-resolution albedos. Nevertheless, it still requires validation via more research and applications outside the boreal biome.

Results so far reveal the possibility of using the stand age as a proxy in climate modelling, not only for albedo dynamics, but also for C dynamics and potentially for more complex biogeochemical and biophysical processes in forest succession – at least for the studied time scale of 5-211 years stand age. Though, this approach carries the risk of neglecting effects of natural disturbances that alter the C and albedo dynamics, e.g. fires or beetle outbreaks. The data clearly indicate a higher relative importance of C-flux compared to albedo-changes in climate effects of the Krycklan catchment. However, more detailed research is needed to understand underlying mechanisms and optimize methodological assumptions (e.g., the reference albedo). The observations are missing the snow-covered period to some extent. Thus, they could serve as a prediction for future patterns where – due to climate change – less snow is present in boreal forests.

Following this approach, the findings point towards a reducing relative importance of albedo in boreal Scandinavia with ongoing climate change and less snow coverage compared to past and current snow cover regimes. Concluding from this, afforestation might become a more valuable climate change mitigation tool also for this biome, especially as snow-fall periods decrease. Generally, the climate benefits of the studied boreal forest are lower when taking albedo into account – independently of the relative importance of albedo. This indicated a more holistic picture, compared to judging the climate effects of forests solely on their C dynamics. Nevertheless, the picture is still incomplete and requires more research on other biogeochemical and biophysical climate variables like evapotranspiration and cloud feedbacks as well as forest-aerosol feedbacks.

The need for more research becomes even more urgent in the light of a changing climate and thus altered forest-climate feedbacks (Thom et al., 2017). An environmental economic analysis points towards a reduced optimum rotation period – compared to a carbon-only approach – for maximum climate benefits in boreal forests when taking albedo-effects into account (Thompson et al. 2009), though more analysis would be needed to clarify this with the produced data. The conclusions suggest including albedo aspects in forest management plans, possibly via C-equivalent emissions in environmental economic analysis and biome-specific incentives for forestry practices (Thompson et al. 2009). More broadly, this study stresses the need to establish a more holistic approach of forests as C sink – not only in science, but also in forestation frameworks.

References

Amiro, B.D., Orchansky, A.L., Barr, A.G., Black, T.A., Chambers, S.D., III, F.S.C., Goulden, M.L., Litvak, M., Liu, H.P., McCaughey, J.H., McMillan, A. & Randerson, J.T. (2006). The effect of post-fire stand age on the boreal forest energy balance. *Agricultural and Forest Meteorology*, 140 (1), 41–50. https://doi.org/10.1016/j.agrformet.2006.02.014

Anderson, R.G., Canadell, J.G., Randerson, J.T., Jackson, R.B., Hungate, B.A., Baldocchi, D.D., Ban-Weiss, G.A., Bonan, G.B., Caldeira, K., Cao, L., Diffenbaugh, N.S., Gurney, K.R., Kueppers, L.M., Law, B.E., Luyssaert, S. & O'Halloran, T.L. (2011). Biophysical considerations in forestry for climate protection. *Frontiers in Ecology and the Environment*, 9 (3), 174–182. https://doi.org/10.1890/090179

Besnard, S., Carvalhais, N., Arain, M.A., Black, A., de Bruin, S., Buchmann, N., Cescatti, A., Chen, J., Clevers, J.G.P.W., Desai, A.R., Gough, C.M., Havrankova, K., Herold, M., Hörtnagl, L., Jung, M., Knohl, A., Kruijt, B., Krupkova, L., Law, B.E., Lindroth, A., Noormets, A., Roupsard, O., Steinbrecher, R., Varlagin, A., Vincke, C. & Reichstein, M. (2018). Quantifying the effect of forest age in annual net forest carbon balance. *Environmental Research Letters*, 13 (12), 124018. https://doi.org/10.1088/1748-9326/aaeaeb

Bonan, G.B. (2008). Forests and Climate Change: Forcings, Feedbacks, and the Climate Benefits of Forests. *Science*, 320 (5882), 1444–1449. https://doi.org/10.1126/science.1155121

Bond-Lamberty, B., Wang, C. & Gower, S.T. (2004). Net primary production and net ecosystem production of a boreal black spruce wildfire chronosequence. *Global Change Biology*, 10 (4), 473–487. https://doi.org/10.1111/j.1529-8817.2003.0742.x

Bright, R.M., Zhao, K., Jackson, R.B. & Cherubini, F. (2015). Quantifying surface albedo and other direct biogeophysical climate forcings of forestry activities. *Global Change Biology*, 21 (9), 3246–3266. https://doi.org/10.1111/gcb.12951

Burakowski, E.A., Ollinger, S.V., Lepine, L., Schaaf, C.B., Wang, Z., Dibb, J.E., Hollinger, D.Y., Kim, J., Erb, A. & Martin, M. (2015). Spatial scaling of reflectance and surface albedo over a mixed-use, temperate forest landscape during snow-covered periods. *Remote Sensing of Environment*, 158, 465–477. https://doi.org/10.1016/j.rse.2014.11.023

Cherubini, F., Santaniello, F., Hu, X., Sonesson, J., Stromman, A.H., Weslien, J., Djupstrom, L.B. & Ranius, T. (2018). Climate impacts of retention forestry in a Swedish boreal pine forest. *Journal of Land Use Science*, 13 (3), 301–318. https://doi.org/10.1080/1747423X.2018.1529831

Coursolle, C., Margolis, H.A., Giasson, M.-A., Bernier, P.-Y., Amiro, B.D., Arain, M.A., Barr, A.G., Black, T.A., Goulden, M.L., McCaughey, J.H., Chen, J.M., Dunn, A.L., Grant, R.F. & Lafleur, P.M. (2012). Influence of stand age on the magnitude and seasonality of carbon fluxes in Canadian forests.

Agricultural and Forest Meteorology, 165, 136–148. https://doi.org/10.1016/j.agrformet.2012.06.011

Curtis, P.S. & Gough, C.M. (2018). Forest aging, disturbance and the carbon cycle. *New Phytologist*, 219 (4), 1188–1193. https://doi.org/10.1111/nph.15227

Felton, A., Löfroth, T., Angelstam, P., Gustafsson, L., Hjältén, J., Felton, A.M., Simonsson, P., Dahlberg, A., Lindbladh, M., Svensson, J., Nilsson, U., Lodin, I., Hedwall, P.O., Sténs, A., Lämås, T., Brunet, J., Kalén, C., Kriström, B., Gemmel, P. & Ranius, T. (2020). Keeping pace with forestry: Multi-scale conservation in a changing production forest matrix. *Ambio*, 49 (5), 1050–1064. https://doi.org/10.1007/s13280-019-01248-0

Fernández-Martínez, M., Vicca, S., Janssens, I.A., Sardans, J., Luyssaert, S., Campioli, M., Chapin III, F.S., Ciais, P., Malhi, Y., Obersteiner, M., Papale, D., Piao, S.L., Reichstein, M., Rodà, F. & Peñuelas, J. (2014). Nutrient availability as the key regulator of global forest carbon balance. *Nature Climate Change*, 4 (6), 471–476. https://doi.org/10.1038/nclimate2177

Frolking, S., Roulet, N.T. (2007). Holocene radiative forcing impact of northern peatland carbon accumulation and methane emissions. *Global Change Biology*, 13 (5), 1079–1088. https://doi.org/10.1111/j.1365-2486.2007.01339.x

Hadden, D. & Grelle, A. (2016). Changing temperature response of respiration turns boreal forest from carbon sink into carbon source. *Agricultural and Forest Meteorology*, 223, 30–38. https://doi.org/10.1016/j.agrformet.2016.03.020

Halim, M.A., Chen, H.Y.H. & Thomas, S.C. (2019). Stand age and species composition effects on surface albedo in a mixedwood boreal forest. *BIOGEOSCIENCES*, 16 (22), 4357–4375. https://doi.org/10.5194/bg-16-4357-2019

He, T., Liang, S., Wang, D., Cao, Y., Gao, F., Yu, Y. & Feng, M. (2018). Evaluating land surface albedo estimation from Landsat MSS, TM, ETM+, and OLI data based on the unified direct estimation approach. *Remote Sensing of Environment*, 204, 181–196. https://doi.org/10.1016/j.rse.2017.10.031

Jackson, R., Randerson, J., Canadell, J., Anderson, R., Avissar, R., Baldocchi, D., Bonan, G., Caldeira, K., Diffenbaugh, N., Field, C., Hungate, B., Jobbágy, E., Kueppers, L., Nosetto, M. & Pataki, D. (2008). Protecting climate with forests. *Environmental Research Letters*, 3. https://doi.org/10.1088/1748-9326/3/4/044006

Janssens, I.A., Dieleman, W., Luyssaert, S., Subke, J.-A., Reichstein, M., Ceulemans, R., Ciais, P., Dolman, A.J., Grace, J., Matteucci, G., Papale, D., Piao, S.L., Schulze, E.-D., Tang, J. & Law, B.E. (2010). Reduction of forest soil respiration in response to nitrogen deposition. *Nature Geoscience*, 3 (5), 315–322. https://doi.org/10.1038/ngeo844

Kalliokoski, T., Bäck, J., Boy, M., Kulmala, M., Kuusinen, N., Mäkelä, A., Minkkinen, K., Minunno, F., Paasonen, P., Peltoniemi, M., Taipale, D., Valsta, L., Vanhatalo, A., Zhou, L., Zhou, P. & Berninger, F. (2020). Mitigation Impact of Different Harvest Scenarios of Finnish Forests That Account for Albedo, Aerosols, and Trade-Offs of Carbon Sequestration and Avoided Emissions. *Frontiers in Forests and Global Change*, 3. https://doi.org/10.3389/ffgc.2020.562044

Kellomaki, S., Strandman, H., Kirsikka-Aho, S., Kirschbaum, M.U.F. & Peltola, H. (n.d.). Effects of thinning intensity and rotation length on albedo- and carbon stock-based radiative forcing in boreal Norway spruce stands. *Forestry*. https://doi.org/10.1093/forestry/cpac058

Kellomäki, S., Väisänen, H., Kirschbaum, M., Kirsikka-Aho, S. & Peltola, H. (2021). Effects of different management options of Norway spruce on radiative forcing through changes in carbon stocks and albedo. *Forestry: An*

International Journal of Forest Research, 94, 588–597. https://doi.org/10.1093/forestry/cpab010

Kirschbaum, M., Whitehead, D., Dean, S., Beets, P., Shepherd, J. & Ausseil, A.-G. (2011). Implications of albedo changes following afforestation on the benefits of forests as carbon sinks. *Biogeosciences*, 8, 8563–8589. https://doi.org/10.5194/bgd-8-8563-2011

Kulmala, M., Suni, T., Lehtinen, K.E.J., Dal Maso, M., Boy, M., Reissell, A., Rannik, Ü., Aalto, P., Keronen, P., Hakola, H., Bäck, J., Hoffmann, T., Vesala, T. & Hari, P. (2004). A new feedback mechanism linking forests, aerosols, and climate. *Atmospheric Chemistry and Physics*, 4 (2), 557–562. https://doi.org/10.5194/acp-4-557-2004

Kuusinen, N., Tomppo, E., Shuai, Y. & Berninger, F. (2014). Effects of forest age on albedo in boreal forests estimated from MODIS and Landsat albedo retrievals. *Remote Sensing of Environment*, 145, 145–153. https://doi.org/10.1016/j.rse.2014.02.005

Landry, J.-S., Parrott, L., Price, D.T., Ramankutty, N. & Matthews, H.D. (2016). Modelling long-term impacts of mountain pine beetle outbreaks on merchantable biomass, ecosystem carbon, albedo, and radiative forcing. *Biogeosciences*, 13 (18), 5277–5295. https://doi.org/10.5194/bg-13-5277-2016

Laudon, H., Hasselquist, E.M., Peichl, M., Lindgren, K., Sponseller, R., Lidman, F., Kuglerová, L., Hasselquist, N.J., Bishop, K., Nilsson, M.B. & Ågren, A.M. (2021). Northern landscapes in transition: Evidence, approach and ways forward using the Krycklan Catchment Study. *Hydrological Processes*, 35 (4), e14170. https://doi.org/10.1002/hyp.14170

Li, Y., Zhao, M., Motesharrei, S., Mu, Q., Kalnay, E. & Li, S. (2015). Local cooling and warming effects of forests based on satellite observations. *Nature Communications*, 6 (1), 6603. https://doi.org/10.1038/ncomms7603

Li, Z., Erb, A., Sun, Q., Liu, Y., Shuai, Y., Wang, Z., Boucher, P. & Schaaf, C. (2018). Preliminary assessment of 20-m surface albedo retrievals from sentinel-2A surface reflectance and MODIS/VIIRS surface anisotropy measures. *Remote Sensing of Environment*, 217, 352–365. https://doi.org/10.1016/j.rse.2018.08.025

Liang, S. & Wang, J. (eds) (2020). Chapter 6 - Broadband albedo. In: *Advanced Remote Sensing (Second Edition)*. Second Edition. Academic Press. 193–250. https://doi.org/10.1016/B978-0-12-815826-5.00006-4

Lin, X., Wu, S., Chen, B., Lin, Z., Yan, Z., Chen, X., Yin, G., You, D., Wen, J., Liu, Q., Xiao, Q., Liu, Q. & Lafortezza, R. (2022). Estimating 10-m land surface albedo from Sentinel-2 satellite observations using a direct estimation approach with Google Earth Engine. *ISPRS Journal of Photogrammetry and Remote Sensing*, 194, 1–20. https://doi.org/10.1016/j.isprsjprs.2022.09.016

Lindroth, A., Holst, J., Linderson, M.-L., Aurela, M., Biermann, T., Heliasz, M., Chi, J., Ibrom, A., Kolari, P., Klemedtsson, L., Krasnova, A., Laurila, T., Lehner, I., Lohila, A., Mammarella, I., Mölder, M., Löfvenius, M.O., Peichl, M., Pilegaard, K., Soosaar, K., Vesala, T., Vestin, P., Weslien, P. & Nilsson, M. (2020). Effects of drought and meteorological forcing on carbon and water fluxes in Nordic forests during the dry summer of 2018. *Philosophical Transactions of the Royal Society B: Biological Sciences*, 375 (1810), 20190516. https://doi.org/10.1098/rstb.2019.0516

Lohila, A., Minkkinen, K., Laine, J., Savolainen, I., Tuovinen, J.-P., Korhonen, L., Laurila, T., Tietavainen, H. & Laaksonen, A. (2010). Forestation of boreal peatlands: Impacts of changing albedo and greenhouse gas fluxes on radiative forcing. *Journal of Geophysical Research - Biogeosciences* 115. https://doi.org/10.1029/2010JG001327

Lucht, W., Schaaf, C. & Strahler, A.H. (2000). An algorithm for the retrieval of albedo from space using semiempirical BRDF models. *IEEE Trans. Geosci. Remote. Sens.*, 38, 977–998

Lukes, P., Stenberg, P. & Rautiainen, M. (2013). Relationship between forest density and albedo in the boreal zone. *Ecological Modelling*, 261, 74–79. https://doi.org/10.1016/j.ecolmodel.2013.04.009

Martínez-García, E., Nilsson, M.B., Laudon, H., Lundmark, T., Fransson, J.E.S., Wallerman, J. & Peichl, M. (2022). Overstory dynamics regulate the spatial variability in forest-floor CO2 fluxes across a managed boreal forest landscape. *Agricultural and Forest Meteorology*, 318, 108916. https://doi.org/10.1016/j.agrformet.2022.108916

Mykleby, P.M., Snyder, P.K. & Twine, T.E. (2017). Quantifying the trade-off between carbon sequestration and albedo in midlatitude and high-latitude North American forests. *Geophysical Research Letters*, 44 (5), 2493–2501. https://doi.org/10.1002/2016GL071459

Myneni, R.B., Dong, J., Tucker, C.J., Kaufmann, R.K., Kauppi, P.E., Liski, J., Zhou, L., Alexeyev, V. & Hughes, M.K. (2001). A large carbon sink in the woody biomass of Northern forests. *Proceedings of the National Academy of Sciences*, 98 (26), 14784–14789. https://doi.org/10.1073/pnas.261555198

Ni, W. & Woodcock, C. (2000). Effect of canopy structure and the presence of snow on the albedo of boreal conifer forests. *Journal of Geophysical Research - Atmospheres*, 105 (D9), 11879–11888. https://doi.org/10.1029/1999JD901158

Nicodemus, F.E., Richmond, J.C., Hsia, J.J., Ginsberg, I.W. & Limperis, T. (1977). Geometrical considerations and nomenclature for reflectance

O'Halloran, T.L., Law, B.E., Goulden, M.L., Wang, Z., Barr, J.G., Schaaf, C., Brown, M., Fuentes, J.D., Göckede, M., Black, A. & Engel, V. (2012). Radiative forcing of natural forest disturbances. *Global Change Biology*, 18 (2), 555–565. https://doi.org/10.1111/j.1365-2486.2011.02577.x

Pan, Y., Birdsey, R.A., Fang, J., Houghton, R., Kauppi, P.E., Kurz, W.A., Phillips, O.L., Shvidenko, A., Lewis, S.L., Canadell, J.G., Ciais, P., Jackson, R.B., Pacala, S.W., McGuire, A.D., Piao, S., Rautiainen, A., Sitch, S. & Hayes, D. (2011). A Large and Persistent Carbon Sink in the World's Forests. *Science*, 333 (6045), 988–993. https://doi.org/10.1126/science.1201609

Peichl, M., Martínez-García, E., Fransson, J.E.S., Wallerman, J., Laudon, H., Lundmark, T. & Nilsson, M.B. (2023b). On the uncertainty in estimates of the carbon balance recovery time after forest clear-cutting. *Global Change Biology*, n/a (n/a). https://doi.org/10.1111/gcb.16772

Ranabhat, K., Patrikeev, L., Revina, A., Andrianov, K., Lapshinsky, V. & Sofronova, E. (2016). An introduction to solar cell technology. *Istrazivanja i projektovanja za privredu*, 14, 481–491. https://doi.org/10.5937/jaes14-10879

Roujean, J.-L., Leroy, M. & Deschamps, P.-Y. (1992). A bidirectional reflectance model of the Earth's surface for the correction of remote sensing data. *Journal of Geophysical Research: Atmospheres*, 97 (D18), 20455–20468. https://doi.org/10.1029/92JD01411

Schaepman-Strub, G., Schaepman, M.E., Painter, T.H., Dangel, S. & Martonchik, J.V. (2006). Reflectance quantities in optical remote sensing—definitions and case studies. *Remote Sensing of Environment*, 103 (1), 27–42. https://doi.org/10.1016/j.rse.2006.03.002

Shuai, Y., Masek, J.G., Gao, F. & Schaaf, C.B. (2011). An algorithm for the retrieval of 30-m snow-free albedo from Landsat surface reflectance and MODIS BRDF. *Remote Sensing of Environment*, 115 (9), 2204–2216. https://doi.org/10.1016/j.rse.2011.04.019

Thompson, M.P., Adams, D. & Sessions, J. (2009). Radiative forcing and the optimal rotation age. *Ecological Economics*, 68 (10), 2713–2720. https://doi.org/10.1016/j.ecolecon.2009.05.009

Vestin, P., Mölder, M., Kljun, N., Cai, Z., Hasan, A., Holst, J., Klemedtsson, L. & Lindroth, A. (2020). Impacts of Clear-Cutting of a Boreal Forest on Carbon Dioxide, Methane and Nitrous Oxide Fluxes. *Forests*, 11 (9). https://doi.org/10.3390/f11090961

Vicca, S., Luyssaert, S., Peñuelas, J., Campioli, M., Chapin III, F.S., Ciais, P., Heinemeyer, A., Högberg, P., Kutsch, W.L., Law, B.E., Malhi, Y., Papale, D., Piao, S.L., Reichstein, M., Schulze, E.D. & Janssens, I.A. (2012). Fertile forests produce biomass more efficiently. *Ecology Letters*, 15 (6), 520–526. https://doi.org/10.1111/j.1461-0248.2012.01775.x

Virkkala, A.-M., Natali, S.M., Rogers, B.M., Watts, J.D., Savage, K., Connon, S.J., Mauritz, M., Schuur, E.A.G., Peter, D., Minions, C., Nojeim, J., Commane, R., Emmerton, C.A., Goeckede, M., Helbig, M., Holl, D., Iwata, H., Kobayashi, H., Kolari, P., López-Blanco, E., Marushchak, M.E., Mastepanov, M., Merbold, L., Parmentier, F.-J.W., Peichl, M., Sachs, T., Sonnentag, O., Ueyama, M., Voigt, C., Aurela, M., Boike, J., Celis, G., Chae, N., Christensen, T.R., Bret-Harte, M.S., Dengel, S., Dolman, H., Edgar, C.W., Elberling, B., Euskirchen, E., Grelle, A., Hatakka, J., Humphreys, E., Järveoja, J., Kotani, A., Kutzbach, L., Laurila, T., Lohila, A., Mammarella, I., Matsuura, Y., Meyer, G., Nilsson, M.B., Oberbauer, S.F., Park, S.-J., Petrov, R., Prokushkin, A.S., Schulze, C., St. Louis, V.L., Tuittila, E.-S., Tuovinen, J.-P., Quinton, W., Varlagin, A., Zona, D. & Zyryanov, V.I. (2022). The ABCflux database: Arctic–boreal \chemCO_2 flux observations and ancillary information aggregated to monthly time steps across terrestrial ecosystems. *Earth System Science Data*, 14 (1), 179–208. https://doi.org/10.5194/essd-14-179-2022

Wang, Z., Schaaf, C.B., Sun, Q., Shuai, Y. & Román, M.O. (2018). Capturing rapid land surface dynamics with Collection V006 MODIS BRDF/NBAR/Albedo (MCD43) products. *Remote Sensing of Environment*, 207, 50–64. https://doi.org/10.1016/j.rse.2018.02.001

Wanner, W., Strahler, A.H., Hu, B., Lewis, P., Muller, J.-P., Li, X., Schaaf, C.L.B. & Barnsley, M.J. (1997). Global retrieval of bidirectional reflectance and albedo over land from EOS MODIS and MISR data: Theory and algorithm. *Journal of Geophysical Research: Atmospheres*, 102 (D14), 17143–17161. https://doi.org/10.1029/96JD03295

Wramneby, A., Smith, B. & Samuelsson, P. (2010). Hot spots of vegetation-climate feedbacks under future greenhouse forcing in Europe. *Journal of Geophysical Research: Atmospheres*, 115 (D21). https://doi.org/10.1029/2010JD014307

Xu, R., Li, Y., Teuling, A.J., Zhao, L., Spracklen, D.V., Garcia-Carreras, L., Meier, R., Chen, L., Zheng, Y., Lin, H. & Fu, B. (2022). Contrasting impacts of forests on cloud cover based on satellite observations. *Nature Communications*, 13 (1), 670. https://doi.org/10.1038/s41467-022-28161-7

Popular science summary

Scandinavian forests take up Carbon from the air by storing it in trees and the soil. As a gas, Carbon Dioxide is one of the most important greenhouse gases leading to climate change. Planting and supporting forests reduces the amount of Carbon Dioxide in the air, which leads to cooling and lessens climate change. However, Carbon storage is not the only climate effect that forests have. Due to their darker surfaces, forests take up a high amount of sunlight and thus also lead to a warming.

This study looks at the climate effects of a forest in Northern Sweden that is caused by the uptake of Carbon Dioxide and sun energy. The results show that the surface reflection of sun energy is related to the forest age and development. In this study, the cooling effect of the forest by taking up Carbon Dioxide is much greater than the warming effect by taking up sun energy. The research shows that it is important to shape forest management specifically to the area to reach maximum cooling effects.

Acknowledgements

Appendix 1

The following codes are available on GitHub:
1) code for downloading S2 and MODIS imagery
2) code for estimating albedo based on MODIS BSA/WSA and S2 reflectance
3) code for radiative forcing models

Moreover, the dataset of input and output data can be found on GitHub, too. They include:
1) Excel file containing stand data of the 50 forest plots, including remotely sensed mean albedo data and mean annual NEP data,
2) Excel file containing data of albedos from reference sites (clar-cut and Svartberget),
3) Excel file containing the radiation data over Krycklan,
4) Raster files containing the annual Blue Sky Albedo values,
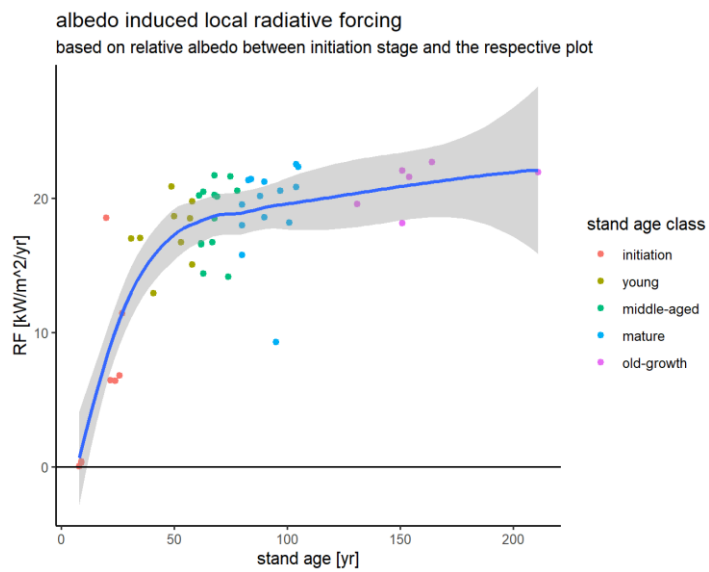5) the locations of the 50 forest plots,
6) shapefile of the catchment outline.

More data and codes can be made available upon request.

The repository can be accessed via: https://github.com/annarequardt/climate-effects-boreal-forests.
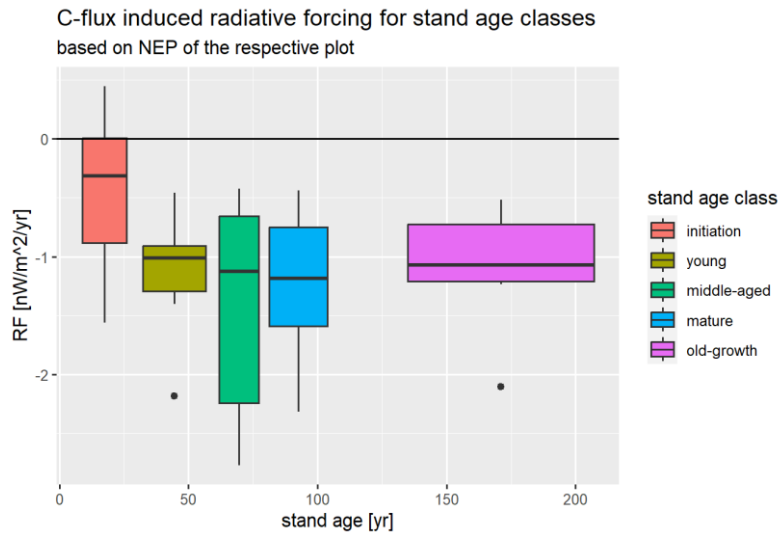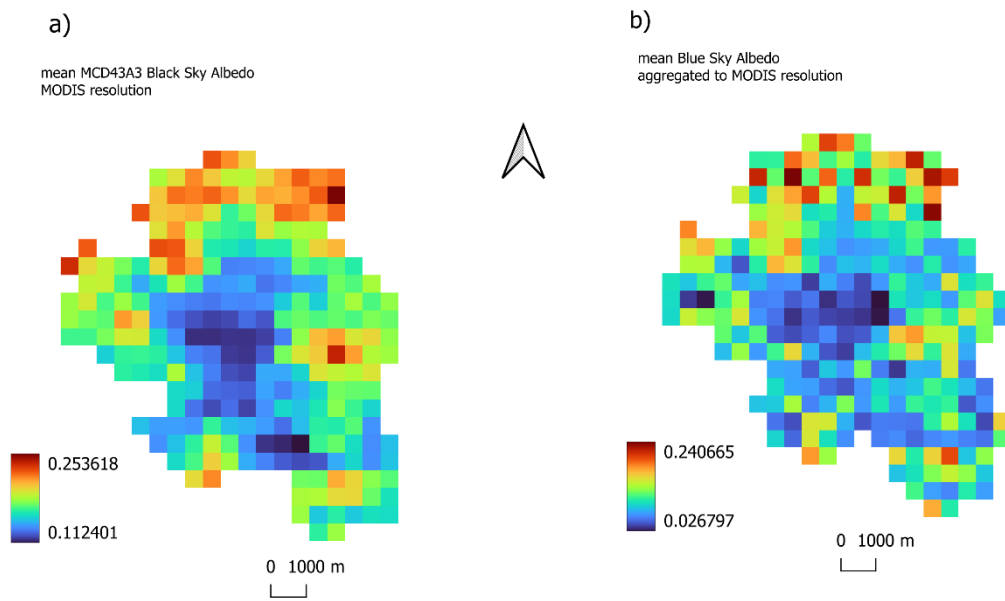
Appendix 2

Appendix 2.1: Boxplot on C-flux induced Radiative forcings for each stand age class, based on the NEP of the respective plots.


Appendix 2.2: Albedo-induced local radiative forcing (not scaled to earth's surface), based on the relative albedo between the initiation stage and the respective plot, grouped by stand age class.
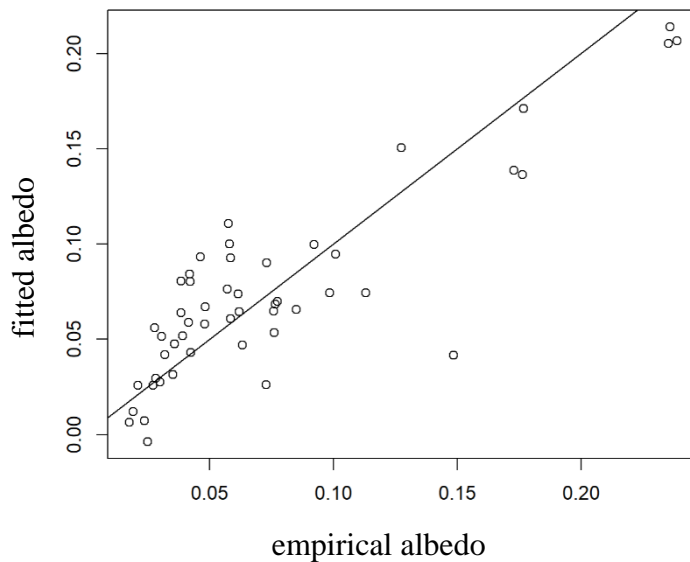
Appendix 3

a)

mean MCD43A3 Black Sky Albedo
MODIS resolution

0.253618

0.112401

0 1000 m

b)

mean Blue Sky Albedo
aggregated to MODIS resolution

0.240665

0.026797

0 1000 m

*Appendix 3: a) mean BSA of the MODIS MCD43A3 product and b) mean Blue Sky Albedo of S2
derived albedo, scaled to MODIS resolution.*

Appendix 4
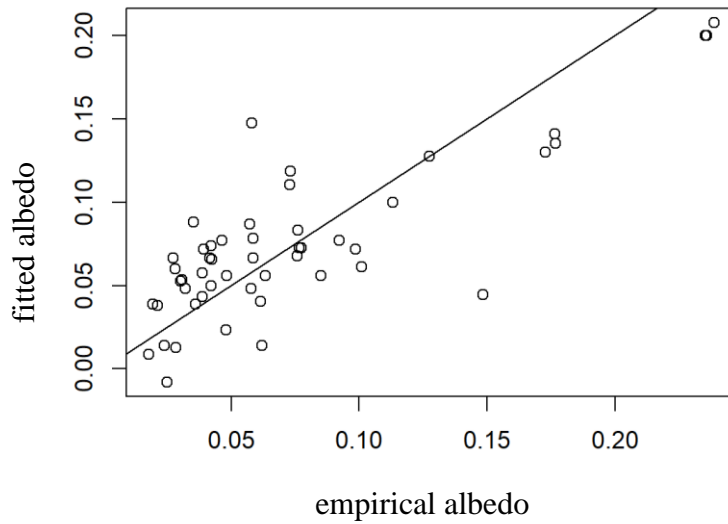
Appendix 4.1: Graphic representation of correlation between fitted albedo values based on the modelled age-albedo relationship and the empirical albedo values.

Appendix 4.2: Graphic representation of correlation between fitted albedo values based on the modelled LAI-albedo relationship and the empirical albedo values.

Publishing and archiving

Approved students' theses at SLU are published electronically. As a student, you have the copyright to your own work and need to approve the electronic publishing. If you check the box for **YES**, the full text (pdf file) and metadata will be visible and searchable online. If you check the box for **NO**, only the metadata and the abstract will be visible and searchable online. Nevertheless, when the document is uploaded it will still be archived as a digital file. If you are more than one author, the checked box will be applied to all authors. You will find a link to SLU's publishing agreement here:

- https://libanswers.slu.se/en/faq/228318.

☒ YES, I/we hereby give permission to publish the present thesis in accordance with the SLU agreement regarding the transfer of the right to publish a work.

☐ NO, I/we do not give permission to publish the present work. The work will still be archived and its metadata and abstract will be visible and searchable.